nature biomedical engineering

SUPPLEMENTARY INFORMATION

https://doi.org/10.1038/s41551-018-0203-4

In the format provided by the authors and unedited.

Low-dose X-ray radiotherapy–radiodynamic therapy via nanoscale metal–organic frameworks enhances checkpoint blockade immunotherapy

Kuangda Lu[1,5], Chunbai He[1,5], Nining Guo[1,2,3,5], Christina Chan[1], Kaiyuan Ni[1], Guangxu Lan[1], Haidong Tang[4], Charles Pelizzari[3], Yang-Xin Fu[4], Michael T. Spiotto[3], Ralph R. Weichselbaum[2,3] and Wenbin Lin[1]*

[1]Department of Chemistry, The University of Chicago, Chicago, IL, USA. [2]The Ludwig Center for Metastasis Research, The University of Chicago, Chicago, IL, USA. [3]Department of Radiation and Cellular Oncology, The University of Chicago, Chicago, IL, USA. [4]Department of Pathology, University of Texas Southwestern Medical Center, Dallas, TX, USA. [5]These authors contributed equally: Kuangda Lu, Chunbai He and Nining Guo.
*e-mail: wenbinlin@uchicago.edu

Materials and Methods

Materials and Animals

All starting materials were purchased from Sigma-Aldrich and Fisher (USA) unless otherwise noted and used without further purification. 1,2-distearoyl-*sn*-glycero-3-phosphoethanolamine-N-[amino(polyethylene glycol)2000] (DSPE-PEG2k) was purchased from Avanti Polar Lipids (USA). 5,10,15,20-tetrabenzoatoporphyrin (H_4TBP) was bought from Porphychem (France). p-terphenyl-4,4”-dicarboxylic acid was bought from Aroz Technologies (USA). Hafnium oxide (HfO_2) nanoparticles were acquired from US Research Nanomaterials, Inc (USA). INCB024360 analogue (IDOi) was purchased from MedKOO Biosciences (USA).

Human head and neck cancer cells SQ20B, JSQ3, SCC61, and HNSCC135, murine breast cancer cell TUBO, and murine prostate cancer cell TRAMP-C2 were donated by Dr. Stephen J. Kron at University of Chicago. Human GBM cells U251 and U87MG and murine GBM cell GL261 were kindly provided by Dr. Maciej S. Lesniak at Northwestern University. Murine colon adenocarcinoma cell CT26 was purchased from the American Type Culture Collection (Rockville, MD, USA). Human colorectal cancer cell HT29, human ovarian cancer cell A2780cisR, human breast cancer cell MCF-7, and human pancreatic cancer cell BxPC-3 were purchased from Developmental Therapeutics Core at Northwestern University. SQ20B, JSQ3, SCC61, and HNSCC135 were cultured in DME/F12 medium (GE Healthcare, USA) supplemented with 20% FBS (Hyclone, USA). TUBO, CT26, and A2780cis were cultured in RPMI 1640 medium (GE Healthcare, USA) supplemented with 10% FBS. TRAMP-C2, U251, U87MG, GL261, MCF-7, and BxPC-3 were cultured in DMEM medium (GE Healthcare, USA) supplemented with 10% FBS. HT29 was cultured in McCoy 5A (Gibco, USA) supplemented with 10% FBS. Mycoplasma was tested before use by MycoAlert detection kit (Lonza Nottingham, Ltd.).

Athymic male and female nude mice (6-8 weeks, 24-26 g) and BALB/c male and female mice (6-8 weeks, 20-22 g) were obtained from Harlan-Envigo Laboratories, Inc (USA). Rag2-/- BALB/c mice were obtained from Taconic Biosciences (USA). The study protocol was reviewed and approved by the Institutional Animal Care and Use Committee (IACUC) at the University of Chicago. Mice requiring veterinary care for any reason were excluded from experiments.

Preparation of DBP-Hf

DBP-Hf was synthesized according to our previous report (K. Lu, C. He, W. Lin, Nanoscale Metal–Organic Framework for Highly Effective Photodynamic Therapy of Resistant Head and Neck Cancer. *J. Am. Chem. Soc.* 136, 16712 (2014)). Briefly, DBP-Hf with the framework formula of $Hf_{12}(\mu_3\text{-}O)_8(\mu_3\text{-}OH)_8(\mu_2\text{-}OH)_6(DBP)_{6.8}(AcO)_{3.5}(OH)_{0.9}(OH_2)_{0.9}$ was synthesized through a solvothermal reaction between $HfCl_4$ and 5,15-di(p-benzoato)-porphyrin (H_2DBP) in N,N-dimethylformamide (DMF) at 80 °C. The resulting dark purple powder was washed with copious amounts of DMF, 1% triethylamine in ethanol (v/v), and ethanol in succession before being dispersed in ethanol as a stock suspension.

Preparation of DBA-Hf

DMF solutions of $HfCl_4$ (5 mL, 1.0 mg/mL, 16 μmol) and 2,5-di(p-benzoato)aniline (H_2DBA, 5mL, 0.9 mg/mL, 14 μmol) were added to a 20 mL glass vial followed by 500 μL of acetic acid. The mixture was kept in a 100 °C oven overnight. The precipitates were removed by centrifugation and the mother liquid was returned to the 100 °C oven for an additional 2 days. The product was collected by centrifugation and washed with DMF, 1% triethylamine in ethanol (v/v), and ethanol.

Preparation of TBP-Hf

To a 2-dram glass vial was added 1 mL of $HfCl_4$ solution [2 mg/mL in N,N-diethylformamide (DEF), 6.2 μmol], 1 mL of the H_4TBP solution (1.9 mg/mL in DEF, 2.4 μmol), and 60 mg of benzoic acid (0.49 mmol). The reaction mixture was kept in a 120 °C oven for 2 days. The violet powder was collected by centrifugation and washed with DMF, 1% triethylamine in ethanol (v/v), and ethanol.

DBP-Hf composition analysis

To a pre-weighed 20-mL glass vial1.0 mL of DBP-Hf ethanolic dispersion was added and oven-dried at 70 °C. After further drying under vacuum, the vial was weighed again to determine the weight of dry MOF. The sample was subjected to the following digestion processes for ICP-MS, UV-vis, NMR, TGA, or powder X-ray diffraction characterization.

ICP-MS (Agilent 7700x, USA) was used to quantify the Hf content in DBP-Hf. The aforementioned dry MOF sample was digested with a mixture of concentrate nitric acid and hydrofluoric acid (HNO_3:HF=99:1 v/v). The digestion is further diluted to appropriate concentration for Hf detection and the concentration was converted to Hf weight percentage in the MOF. The results are listed in Table S1.

The aforementioned dry MOF sample was digested with H_3PO_4/DMSO (85% H_3PO_4:DMSO=5:95 v/v) for UV-vis detection of H_2DBP. The DBP concentration was calculated based on the standard curve of pure ligand at the same condition, and converted to DBP weight percentage in the MOF (**Fig. S2**).

For NMR analysis, the dry MOF sample was digested with 85% D_3PO_4 in DMSO-d_6 (50 μL of D_3PO_4, diluted to 1 mL with DMSO-d_6). The ratio of acetic acid (AcOH) to DBP was determined by the integral of the AcOH peak at δ=1.89 vs. that of the H_2DBP peak at δ=10.69 (**Fig. S3**).

Thermogravimetric analysis was carried out on Shimadzu TGA-50 thermogravimetric analyzer. The sample was heated at 3 °C/min to 800 °C in air. The weight percentage was plotted against temperature (**Fig. S4**). The weight loss before 800 °C was 60.5% (calculated 61.0%).

Powder X-ray diffraction studies were carried out on a Bruker D8 VENTURE Single Crystal Dual-Source Diffractometer. The samples are loaded to a sealed capillary tube and packed with centrifugation before measurements. The model structures were constructed/modified with BIOVIA® Material Studio 7.0.

Single crystal X-ray structure of TBP-Hf

Single crystal X-ray diffraction of TBP-Hf was performed with a Bruker APEX II CCD-based detector at ChemMatCARS (Sector 15), Advanced Photon Source (APS), Argonne National Laboratory. The frames were integrated with the Bruker SAINT© build in APEX II software package using a narrow-frame integration algorithm, which also corrects for the Lorentz and polarization effects. Absorption corrections were applied using SADABS. Structures were solved by direct methods and refined to convergence by least squares method on F^2 using the SHELXTL-2013 software suite.

Due to relatively weak diffraction and low resolution, not uncommon for frameworks with very large solvent accessible void spaces, restraints (RIGU) were applied to displacement parameters. The phenyl ring was constrained to ideal geometry. Non-hydrogen atoms were refined isotropically. SQUEEZE subroutine of the PLATON software suite was applied to remove scattering from the highly disordered guest molecules. The resulting new HKL4 files were used to further refine the structure.

Singlet oxygen generation by 4-nitroso-N,N-dimethylanaline (RNO)

The nMOF samples (DBP-Hf and TBP-Hf) were prepared as aqueous suspensions in the presence of 25 μM of RNO and 10 μM of histidine. The solutions were transferred to 1-dram vials for visible light irradiation or X-ray irradiation. For visible light irradiation, DBP-Hf (0.42 μM) was irradiated by a 630 nm LED (100 mW/cm^2) for 2, 5, 10, 15, 20 and 30 min; TBP-Hf (2.5 μM) was irradiated by a 650 nm LED (100 mW/cm^2) for 1, 2, 5, 10, 15, 20 and 30 min. For X-ray irradiation, DBP-Hf (0.83, 1.67 or 4.17 μM) and TBP-Hf (5 μM) were given X-ray doses of 1, 2, 4 or 8 Gy. The UV-vis absorption spectra of the solutions were taken on a spectrophotometer (**Fig. S11-S12**). The difference in the RNO peak absorbance [Δ(OD)] at 439 nm was calculated by subtracting the readout in the sample curve from that of the control (no irradiation) curve.

PEGylation of DBP-Hf

DBP-Hf (1 mg/mL) in ethanol was mixed with DSPE-PEG$_{2000}$ (5 mg/mL) in THF at DBP-Hf:DSPE-PEG$_{2000}$ weight ratios of 1:1, 1:2, 1:5, and 1:10. The mixed solution was concentrated by a nitrogen flow to 50 μL and then vortexed for 1 min. One milliliter of water was added to this mixed solution. The mixture was vortexed for 1 min and sonicated for 5 min to yield DBP-Hf@PEG.

The particle sizes and polydispersity index (PDI) of DBP-Hf@PEG were determined by dynamic light scattering (DLS) measurements. **Tables S3 and S4** summarize the Z-averages, Number-averages, and PDIs of DBP-Hf@PEG formulated with different weight ratios of nMOF:DSPE-PEG$_{2000}$. The particle sizes and PDIs of DBP-Hf dispersed in ethanol and water at a concentration of 50 μg/mL were also determined for comparison.

The stability of DBP-Hf@PEG was further evaluated in phosphate buffered solution (PBS). DBP-Hf@PEG (50 μg) was centrifuged at 13000 rpm for 15 min. The precipitate was dispersed

in 1 mL of PBS followed by sonication for 5 min. The particle sizes and PDI of DBP-Hf@PEG in PBS were determined by DLS measurements. The particle sizes of DBP-Hf@PEG decreased after being dispersed in PBS compared to those determined in water, likely due to the effects of the salt on the PEG layer.

Biodistribution of DBP-Hf@PEG by intravenous (i.v.) injection

Murine colon carcinoma CT26 cells were subcutaneously injected in the right flanks of BALB/c mice (2 million cells/mouse). After the tumour size reached 100 mm^3 in volume, 200 μL of DBP-Hf@PEG suspension was intravenously injected to the mice at a dose of 37.5 mg/kg. Mice were sacrificed 24 h post injection. Liver, lung, kidney, and tumour tissues were harvested for the determination of Hf concentrations by ICP-MS.

In vivo efficacy of DBP-Hf@PEG by intravenous injection

After the tumours reached a size of 100 mm^3, DBP-Hf@PEG (37.5 mg/kg) was intraveneously injected every five days for a total of two injections, followed by 10 fractions of daily X-ray irradiation (1 Gy/fraction, 120 kVp, 20 mA, 2-mm Cu filter). The tumour size was measured daily with a digital caliper. Tumour volumes were calculated as follows: ($width^2$ × length)/2. When the size of the tumour in the control group reached 2 cm^3, all the mice were sacrificed.

Cellular uptake

The cellular uptake of DBP-Hf and TBP-Hf along with DBA-Hf and HfO_2 nanoparticle controls was evaluated in human HNSCC SQ20B cells. SQ20B cells were seeded on 6-well plates at a density of 10^6 cells /well and cultured for 24 h. DBP-Hf, TBP-Hf, DBA-Hf or HfO_2 nanoparticle was added to the cells at Hf doses of 50 μM. After a 4-h incubation, the cells were collected and counted by a hemocytometer. Concentrated nitric acid was used to digest the cells and the concentrations of metals in the digested cells were determined by ICP-MS.

Cytotoxicity

The acute cytotoxicity of DBP-Hf upon X-ray irradiation was evaluated against ten different human cancer cell lines: four HNSCC (SQ20B, JSQ3, SCC61, HNSCC135), two glioblastoma (GBM, U251, U87), one colon cancer (HT29), one cisplatin-resistant ovarian cancer (OCa, A2780cisR), one breast cancer (MCF-7), and one pancreatic cancer cell (PDAC, BxPC-3). The cytotoxicity of TBP-Hf upon X-ray irradiation was evaluated in murine glioblastoma GL261, human glioblastoma U251 and U87, murine colorectal cancer CT26, murine breast cancer TUBO, murine prostate cancer TRAMP-C2, and human HNSCC SQ20B cells.

Several X-ray irradiation doses ranging from 0-1 Gy were applied to determine the X-ray irradiation dose dependent cytotoxicity. DBP-Hf (at a dose of 0.83 μM) or TBP-Hf (at a dose of 1.67 μM) was incubated with cells for 4 h before the cell culture medium was replaced with fresh medium. The cells were submitted to X-ray irradiation at 250 kVp and 10 mA current and then

incubated for 72 h. Their viability was then determined through an MTS assay. The cytotoxicity of DBA-Hf and HfO_2 nanoparticles at Hf doses of 10 μM induced by X-ray irradiation against SQ20B was evaluated using the same method.

The acute cytotoxicity of DBP-Hf and TBP-Hf induced by X-ray irradiation was compared with that induced by LED light irradiation. DBP-Hf or TBP-Hf was incubated with cells for 4 h before the cell culture medium was replaced with fresh medium. The cells were submitted to X-ray irradiation or LED light irradiation (630 nm for DBP-Hf and PpIX, and 645 nm for TBP-Hf, 100 mW/cm^2, 180 J/cm^2). The X-ray dose required to achieve similar cytotoxicity as 180 J/cm^2 light irradiation was estimated based on the dose-dependent cancer cell killing curve.

The cytotoxicity of DBP-Zr and TBP-Zr particles upon X-ray irradiation were evaluated against human HNSCC SQ20B cells. DBP-Zr or TBP-Zr at doses varying from 0 to 4.17 μM were incubated with cells for 4 h before the cell culture medium was replaced with fresh medium. The cells were submitted to X-ray irradiation at 0 Gy or 1 Gy at 250 kVp and 10 mA current and then incubated for 72 h before determining their viability with an MTS assay.

The tissue penetration of X-ray induced cytotoxicity was evaluated and compared with LED light induced cytotoxicity. DBP-Hf at a dose of 1.67 μM was incubated with SQ20B cells for 4 h before the cell culture medium was replaced with fresh medium. The cells were subjected to X-ray irradiation (0.5 Gy) or LED light irradiation (180 J/cm^2). A piece of beef of 1 cm in thickness or a stack of beef of 4.5 cm in thickness was placed on the cell plate cover during LED light irradiation or X-ray irradiation to mimic deep tumour environments.

Clonogenic assay

The Clonogenic assay was used to evaluate the radiosensitizing effect of HfO_2, DBA-Hf, and DBP-Hf according to modified protocols. Generally, cells were seeded in 6-well plates and cultured for 12 h. After incubated with particles at Hf concentrations of 20 μM for 4 h, cells were irradiated with X-ray at 0, 1, 2, 4, 8 and 16 Gy dose. Cells were trypsinized and counted immediately. For 0, 1, 2, 4 Gy irradiated samples, 200 cells were seeded on 6-well plates and cultured with 2 mL medium for 10-20 days. For 8 Gy and 16 Gy irradiated samples, 1000 and 10000 cells were seeded, respectively. When cell clones were observed, the culture medium was discarded and the plates rinsed with PBS twice. 500 μL of 0.5% crystal violet (50% methanol) were added in each well for staining. The wells were then rinsed with water and the clones were counted. The numbers of clones are converted to survival fraction by normalizing to 0 Gy control groups for each material.

For clonogenic assay post PDT treatment, the cells were incubated in the same manner as above before being irradiated with LED lamp (fluence rate at 100 mW/cm^2) for 2.5, 5, 10 and 15 min. Cells were trypsinized and counted immediately. In each well 200 cells were seeded on 6-well plates and cultured with 2 mL medium for 10-20 days. The cell clones were rinsed, stained and counted using the same method as described above. The numbers of clones were converted to survival fraction by normalizing to dark control groups for each material.

γ-H2AX assay

The double-strand break (DSB) caused by DBP-Hf and TBP-Hf upon irradiation and LED light irradiation was investigated using a HCS DNA Damage Kit (Life Technology, USA) of SQ20B cells. To assess the effects of X-ray irradiation, SQ20B cells were incubated with 0.83 μM DBP-Hf or 1.67 μM TBP-Hf for 4 h, and then irradiated with X-rays at 0, 0.1, 0.5, and 1 Gy. SQ20B cells incubated with PBS and irradiated with 1 Gy X-ray served as a control. To assess the effects of LED light irradiation, SQ20B cells were incubated with 0.83 μM DBP-Hf or 1.67 μM TBP-Hf for 4 h, and then irradiated with LED light for 30 min at a fluence rate of 100 mW/cm^2 (180 J/cm^2). γ-H2AX assays were carried out immediately after X-ray or light irradiation. The nuclei were stained with DAPI. The cells were imaged with CLSM. Red fluorescence indicated the DSBs stained with antibody-labeled γ-H2AX.

Intracellular singlet oxygen ($^1O_2$) generation

$^1O_2$ generation in live cells was detected by Singlet Oxygen Sensor Green (SOSG, Life Technology, USA). SQ20B cells were seeded in a 3.5-cm petri dish and cultured for 24 h. The culture medium was then replaced with fresh medium containing 1 μM SOSG to preload the cells with SOSG. After incubating for 30 min, the cells were washed with PBS three times to remove excess SOSG. The cells were incubated with PBS, 0.83 μM DBP-Hf, or 1.67 μM TBP-Hf for 4 h and then washed with PBS three times to remove excess nMOFs. X-ray irradiation was applied to cells at a dose of 1 Gy. CLSM was used to visualize the $^1O_2$ generated in live cells by detecting the green fluorescence inside the cells.

COX-2 assay

The cell membrane damage caused by RDT upon X-ray was investigated by COX-2 assay (BD Bioscience, USA) in SQ20B cells. Cells were seeded on cover slides in 3.5 cm petri dishes and cultured for 12 h before incubated with particles at Hf concentrations of 10 μM or ligands concentrations of 10 μM for 4 h, followed by X-ray irradiation at 0 and 1 Gy dose. Cells were fixed with 4% paraformaldehyde immediately after X-ray or light irradiation. Biotin-conjugated anti-COX-2 antibody at 10 μg/mL concentration were incubated with cells at 4 °C overnight, followed by incubation with Cy3-conjugated streptavidin. The nuclei were stained with DAPI. The cells were imaged with CLSM.

In vivo anticancer efficacy of DBA-Hf by intratumoural injection

We further evaluated the *in vivo* anticancer efficacy of DBA-Hf by intratumoural injection on CT26 tumour bearing mice. When the tumours reached 100 mm^3 in volume, 0.52 mg DBA-Hf (1.0 nmol Hf) was intratumourally injected, followed by daily X-ray irradiation at a dose of 2 Gy/fraction for a total of 5 fractions on consecutive days.

Biodistribution of DBP-Hf and TBP-Hf by intratumoural injection

Murine colon carcinoma CT26 cells were subcutaneously injected to the right flanks of BALB/c mice (2 million cells/mouse). After the tumour size reached 100 mm^3 in volume, a

suspension of 0.15 mg DBP-Hf or 0.60 mg TBP-Hf was intratumourally injected to the mice. Mice were sacrificed right after injection or 12 h post injection. Mice received X-ray irradiation at 2 Gy at the tumour site 12 h post injection and then were sacrificed at pre-determined time points. For each group and time point, three mice were sacrificed. Blood, heart, liver, spleen, lung, kidney, and bladder were harvested for the determination of Hf concentrations by ICP-MS. The tumours were harvested and homogenized with saturated K_3PO_4. DBP or TBP ligand was further extracted by DMSO followed by centrifugation. The supernatant was subjected to UV-vis to determine the ligand concentration in the tumours. The precipitate was lyophilized, digested by concentrated nitric acid, and subjected to ICP-MS to determine the Hf concentrations in the tumours.

T cell and B cell depletion

The anticancer efficacy of DBP-Hf was evaluated using a subcutaneous TUBO model in BALB/c mice with T cell or B cell depletion. When tumours reached ~100 mm^3 in volume, 0.15 mg of DBP-Hf was intratumourally injected to the mice. Anti-CD4 (for CD4+ T cell depletion), anti-CD8 (for CD8+ T cell depletion), anti-CD20 (for B cell depletion), or mouse IgG (control) were intraperitoneally injected into the mice (200 μg/mouse/injection) on Days 0 and 5 after the first treatment. Twelve hours post-injection, mice were anesthetized with 2% (v/v) isoflurane, and tumours were irradiated with image-guided X-ray at 225 kVp, 13 mA, 0.3-mm Cu filter. The nMOFs were injected every three days, for a total of two injections, and then irradiated daily with X-rays on six consecutive days at dose of 0.5 Gy/fraction. To evaluate the therapeutic efficacy, tumour growth and bodyweight evolution were monitored. The tumour size was measured with a digital caliper every day. Tumour volumes were calculated as follows: $(\text{width}^2 \times \text{length})/2$.

Preparation and characterization of IDOi@DBP-Hf

To a 2-dram glass vial was added 2.28 mg of IDOi (8.4 μmol) and 1.0 mL of DBP-Hf suspension (2.0 mg/mL in ethanol). After dissolution of IDOi with the help of sonication, 1.0 mL of water was added. The mixture was stirred in the dark for 12 hours. The loaded nMOF was collected by centrifugation and washed with 50% ethanol/water (v/v).

Thermogravimetric analysis (TGA) was carried out on DBP-Hf samples before and after IDOi loading on Shimadzu TGA-50 thermogravimetric analyzer. Heating speed was set to 3 °C/min and the sample was heated to 700 °C in air. The weight percentage was plotted against the temperature. Pure IDOi has a weight loss of ~90% at ~200 °C. The drug loading was calculated to be 9.4% by weight following the equation below:

$$loading\ wt\% = \left(1 - \frac{remaining\ wt\%\ after\ loading}{remaining\ wt\%\ before\ loading}\right) \times 100\%$$

Determination of Tryptophan and Kynurenine by LC-MS

The plasma concentrations of Tryptophan (Trp) and Kynurenine (Kyn) were determined by LC-MS after extraction as follows:

To 100 μL plasma samples were added Trp 100 ppm + Kyn 1 ppm as external standards (0, 20, 40, 80 μL). 900 μL of methanol was added to the samples to precipitate the protein. The

samples were then vortexed for 1 min, sonicated for 1 min, and cooled in a 4 ºC refrigerator. The samples were then centrifuged at 10000 rpm for 10 min. The pellet was further extracted with another 500 μL of methanol using the same method, and the methanol extractions were combined. The solvents were evaporated with a nitrogen stream, and the samples were then further dried under a vacuum. 400 μL of methanol was added to each sample to dissolve the substrates, and the solution was filtered through a 200 nm PTFE filtering unit. The samples were subjected to LC-MS to quantify Kyn and Trp.

The LC-MS protocol is as follows:

- Column: Agilent Zorbax SB-C18 (50 × 2.1mm, 5 μm)
- Injection: 10 μL
- Solvent A: 0.2% formic acid in water, v/v
- Solvent B: acetonitrile
- Flow rate: 0.3 mL/min
- ESI mode: positive
- Fragmentor voltage: 90 V for all three compounds
- Samples solution in methanol
- Initial time 0: 100% A, 0% B
  At 1.5 min, set 100% A, 0% B
  At 3.0 min, set 60% A, 40% B
  At 7.0 min, set 60% A, 40% B
  At 7.5 min, set 100% A, 0% B
  At 9 min, set 100% A, 0% B

Determination of IDOi by LC-MS

Tumours were established by subcutaneous inoculation of TUBO cell suspension into both flanks of the mice (2×10^6 cells per mouse into the right flank region and 4×10^5 cells per mouse into the left flank region). When right tumours reached 100-150 mm^3, IDOi@DBP-Hf was intratumourally injected into the right tumour (DBP-Hf 0.11 mg, IDOi 0.56 mg/kg). Eight hours post IDOi@DBP-Hf injection, the mice were sacrificed and the whole blood and tumours were collected for IDOi quantification.

Both side tumours and blood samples (200 μL for each mouse) were homogenized in 1 mL of methanol. The precipitates were separated by centrifugation and extracted with 1 mL of methanol for one more time. The methanol extracts of each sample were combined, dried under vacuum, reconstituted in methanol (1 mL for right tumours and 0.5 mL for blood and left tumours), and filtered through 0.22 μm PTFE filter units, and then used for LC-MS quantification.

Abscopal effect of IDOi@DBP-Hf on TUBO tumour bearing Rag2-/- mice

The abscopal effect of IDOi@DBP-Hf was evaluated using a subcutaneous TUBO model in Rag2-/- BALB/c mice. The bilateral tumour model was established as described above. Two groups were included for comparison: (1) PBS + 0.5 Gy (2) IDOi@DBP-Hf 0.15 mg DBP-Hf and 0.78 mg/kg IDOi + 0.5 Gy. When tumours reached 100-150 mm^3 in volume, IDOi@DBP-Hf or

PBS was intratumourally injected into the mice. Twelve hours post-injection, mice were anesthetized with 2% (v/v) isoflurane, and their tumours were irradiated with an image-guided X-ray at 225 kVp, 13 mA, 0.3-mm Cu filter. The nMOFs were injected every three days, for a total of two injections, followed by daily X-ray irradiations on six consecutive days at a dose of 0.5 Gy/fraction. To evaluate the therapeutic efficacy, tumour growth and bodyweight evolution were monitored. Tumour sizes were measured with a digital caliper every day. Tumour volumes were calculated as follows: $(\text{width}^2 \times \text{length})/2$.

Apoptosis assay

The apoptosis induced by RT-RDT treatment was determined by flow cytometry using an Alexa Fluor 488 Annexin V/dead cell apoptosis kit. No apoptosis or necrosis was observed for cells treated with DBP-Hf or PBS in the dark, while significant numbers of cells underwent apoptosis when treated with DBP-Hf upon X-ray irradiation at the dose of 2 Gy.

CRT assay

The immunogenic cell death (ICD) induced by DBP-Hf radiation treatment was investigated by detecting cell-surface expression of calreticulin (CRT). CT26 cells were seeded in 6-well plates overnight and incubated with DBP-Hf at 10 μM based on Hf concentration for 4 hours followed by treatment of X-ray irradiation at 0 and 2 Gy dose (250 kVp, 15 mA, 1 mm Cu filter). PBS-treated groups served as control. Then cells were cultured in the incubator for another 4 hours before confocal microscopy observations. Cells were stained with DAPI for nuclei and CellMask™ Deep Red (Life Technology, USA) for membrane. Stronger green fluorescence was observed in group treated with DBP-Hf upon X-ray irradiation compared to either PBS treated groups or DBP-Hf treated group without X-ray irradiation under CLSM, indicating immunogenic cell death was induced after DBP-Hf-enabled RT-RDT treatment with low-dose X ray.

Systemic toxicity of DBP-Hf on mice

Balb/c mice (4-6 weeks old and weighing 18-24 g) or C57BL/6 mice (4-6 weeks old and weighing 25-28 g) were subcutaneously injected on the right flank with 5 mL/kg of either phosphate buffered saline (PBS, 3/sex/group) or PBS dispersion of DBP-Hf at 60 mg/kg (3/sex/group). Animals were observed for 14 days for survival and signs of toxicity. Mortality and morbidity checks were conducted daily. Body weights were recorded pre-study and daily thereafter.

No mortality or clinical signs of toxicity was observed, with purple stained fur seen at the injection site. Animal weight gains (**Supplementary Fig. S28**) were similar between the PBS-treated groups and DBP-Hf -treated groups, indicating the lack of acute toxicity in two different strains of mice upon subcutaneous injection of up to 60 mg/kg DBP-Hf.

Systemic toxicity of DBP-Hf on rats

Twenty-four (12/sex) Sprague Dawley rats were randomly assigned to two groups (6 animals/sex per group). Animals were administered control article (1X PBS) or DBP-Hf (63 mg/kg) once weekly on Day 0, 7, 14, and 21 via subcutaneous injection to the mid-scapular region. The rats were evaluated by mortality, physical examinations, cageside observations, body weights, body weight changes, and clinical chemistry. The results shown in **Supplementary Fig. 4g** and **Supplementary Table S13** indicate that DBP-Hf is non-toxic to rats at up to 63 mg/kg.

Distribution of nMOF into normal tissues

Balb/c mice were inoculated with CT26 cells and treated with DBP-Hf (3 mice) or TBP-Hf (3 mice) and X-ray irradiation in accordance with our treatment strategy. After irradiation on the fourth day post treatment, the mice were euthanized and the tumour was carefully excised. Muscle of the right flank directly adjacent to the tumour and muscle of the contralateral left flank were also removed. The tissues were weighed, digested with 1% HF in HNO_3, and subjected to ICP-MS analysis to determine Hf content.

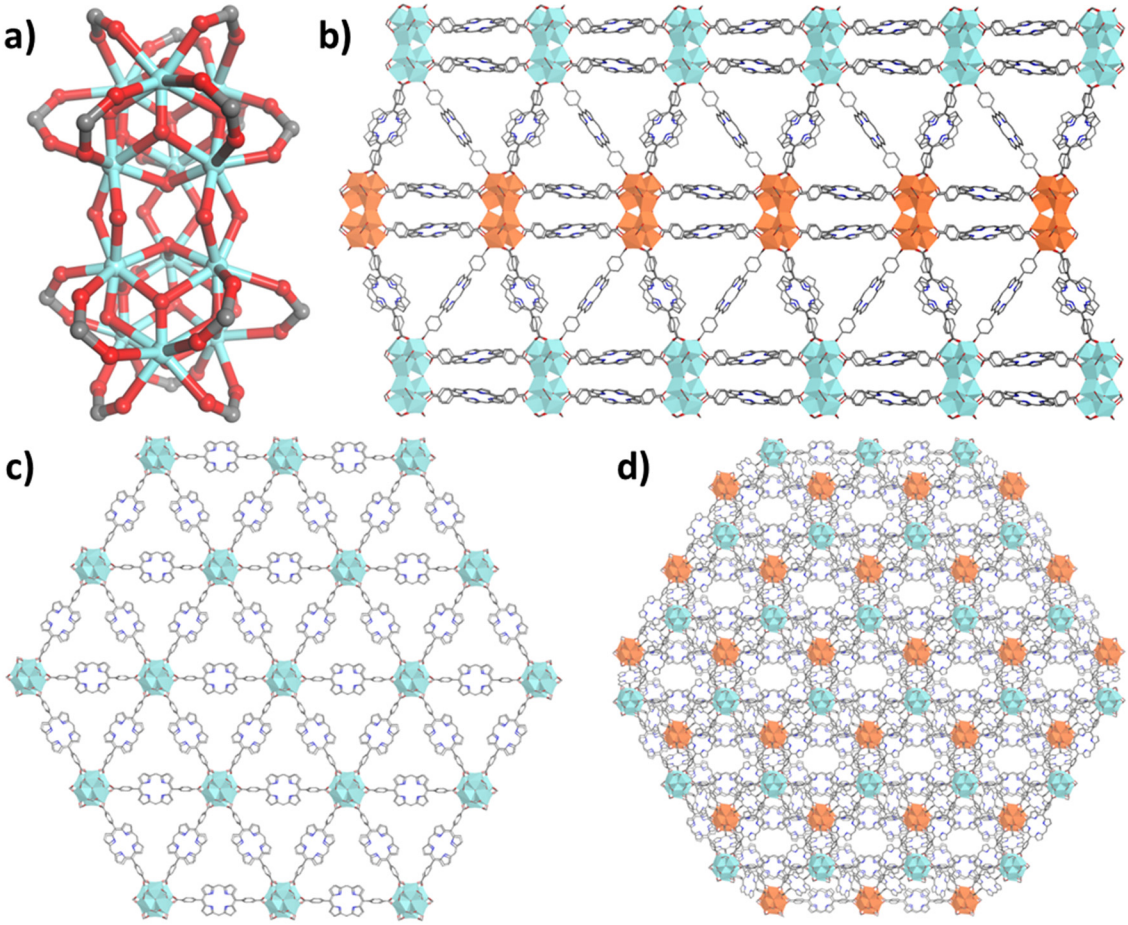

Supplementary Figure 1: Structure model of DBP-Hf. (a) The structure of $Hf_{12}(\mu_3\text{-}O)_8(\mu_3\text{-}OH)_8(\mu_2\text{-}OH)_6(RCO_2)_{18}$ cluster. (b) The side view of nanosheets. Different colors are arbitrarily used to illustrate the packing of the layers in ABAB pattern. Views along *c* axis of the nanosheets showing a single layer (c) or the stack of multiple layers (d). Red: oxygen; gray: carbon; blue: nitrogen; cyan and orange: hafnium.

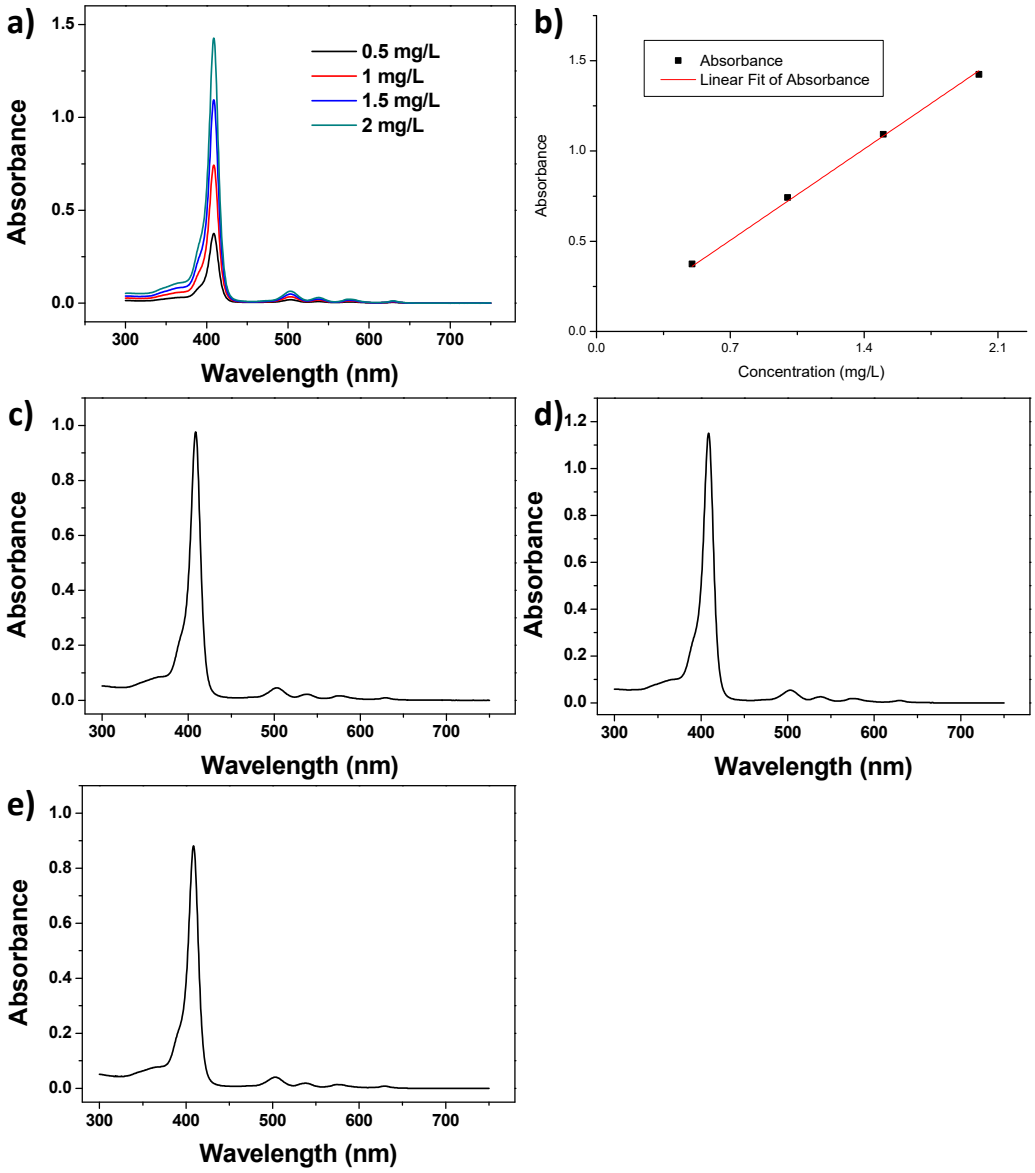

Supplementary Figure 2: UV-vis determination of the DBP content in DBP-Hf. Absorption curves (a) and fitted standard curve (b) of H_2DBP in DMSO. (c-e) Absorption curves of different batches of DBP-Hf after digestion with H_3PO_4/DMSO.

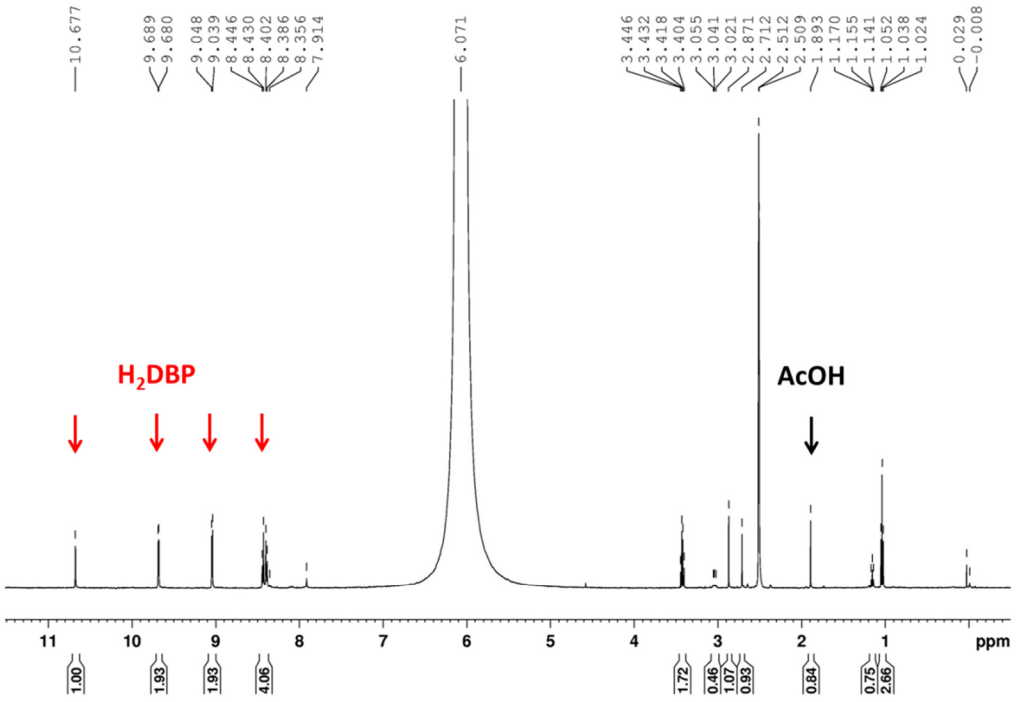
10.677
9.689
9.680
9.048
9.039
8.446
8.430
8.402
8.386
8.356
7.914
6.071
3.446
3.432
3.418
3.404
3.055
3.041
3.021
2.871
2.712
2.512
2.509
1.893
1.170
1.155
1.141
1.052
1.038
1.024
0.029
-0.008
H2DBP
AcOH
11
10
9
8
7
6
5
4
3
2
1
ppm
1.00
1.93
1.93
4.06
1.72
0.46
1.07
0.93
0.84
0.75
2.86

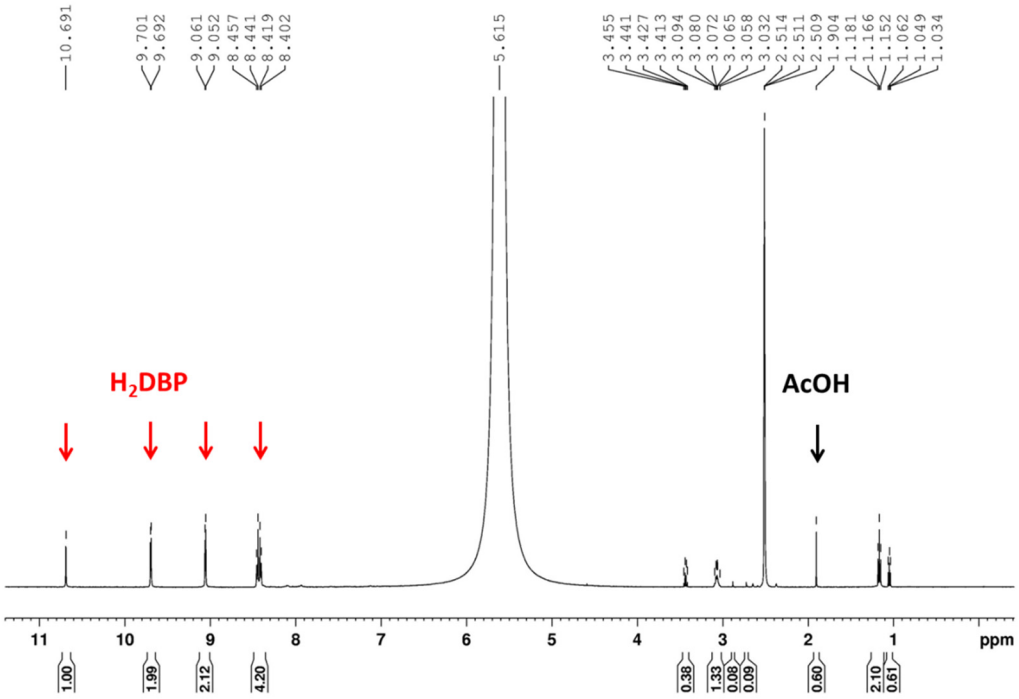
10.691
9.701
9.692
9.061
9.052
8.457
8.441
8.419
8.402
5.615
3.455
3.441
3.427
3.413
3.094
3.080
3.072
3.065
3.058
3.032
2.514
2.511
2.509
1.904
1.181
1.166
1.152
1.062
1.049
1.034
H2DBP
AcOH
11
10
9
8
7
6
5
4
3
2
1
ppm
1.00
1.99
2.12
4.20
0.38
1.33
0.08
0.09
0.60
2.10
0.61

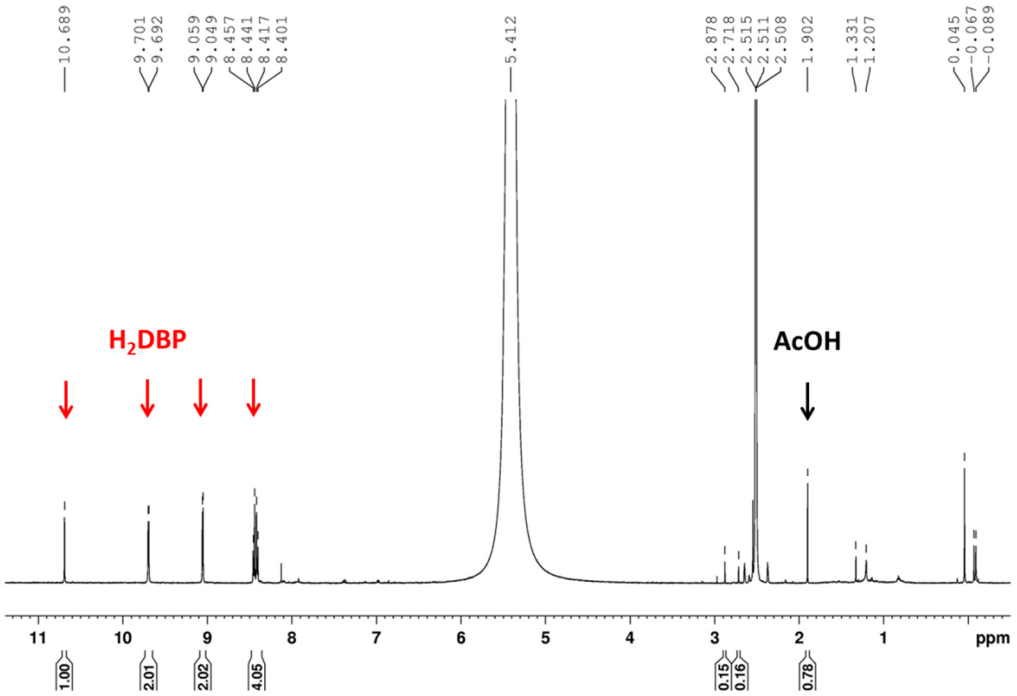

Supplementary Figure 3: ^{1}H NMR spectra for the quantification of the acetic acid content in DBP-Hf. Three different batches were digested with 85% D_3PO_4/DMSO-D_6 and the acetic acid contents were evaluated by the ratios to DBP based on the integrals of the NMR spectra. The ratios are listed in Table S1.

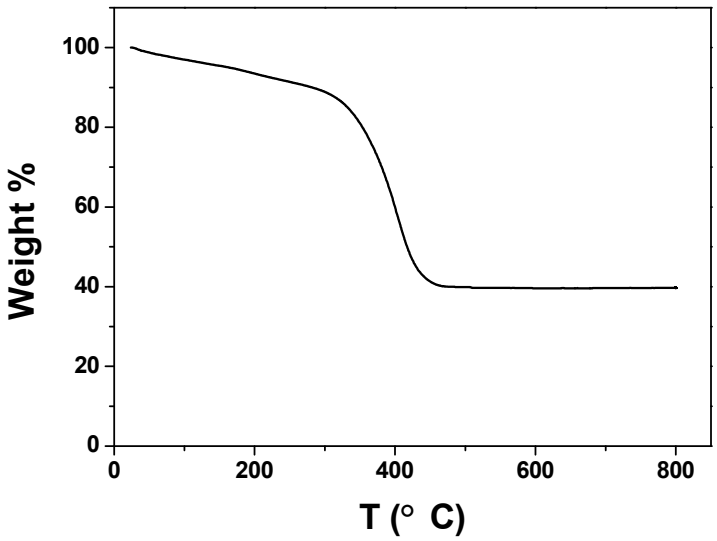

Supplementary Figure 4: Thermogravimetric analysis on DBP-Hf. The sample was dried on vacuum before loaded to the instrument. Calculated remaining weight percentage: 39.0%; experimental remaining weight percentage: 39.5%. One of two independent experiments with similar results is shown.

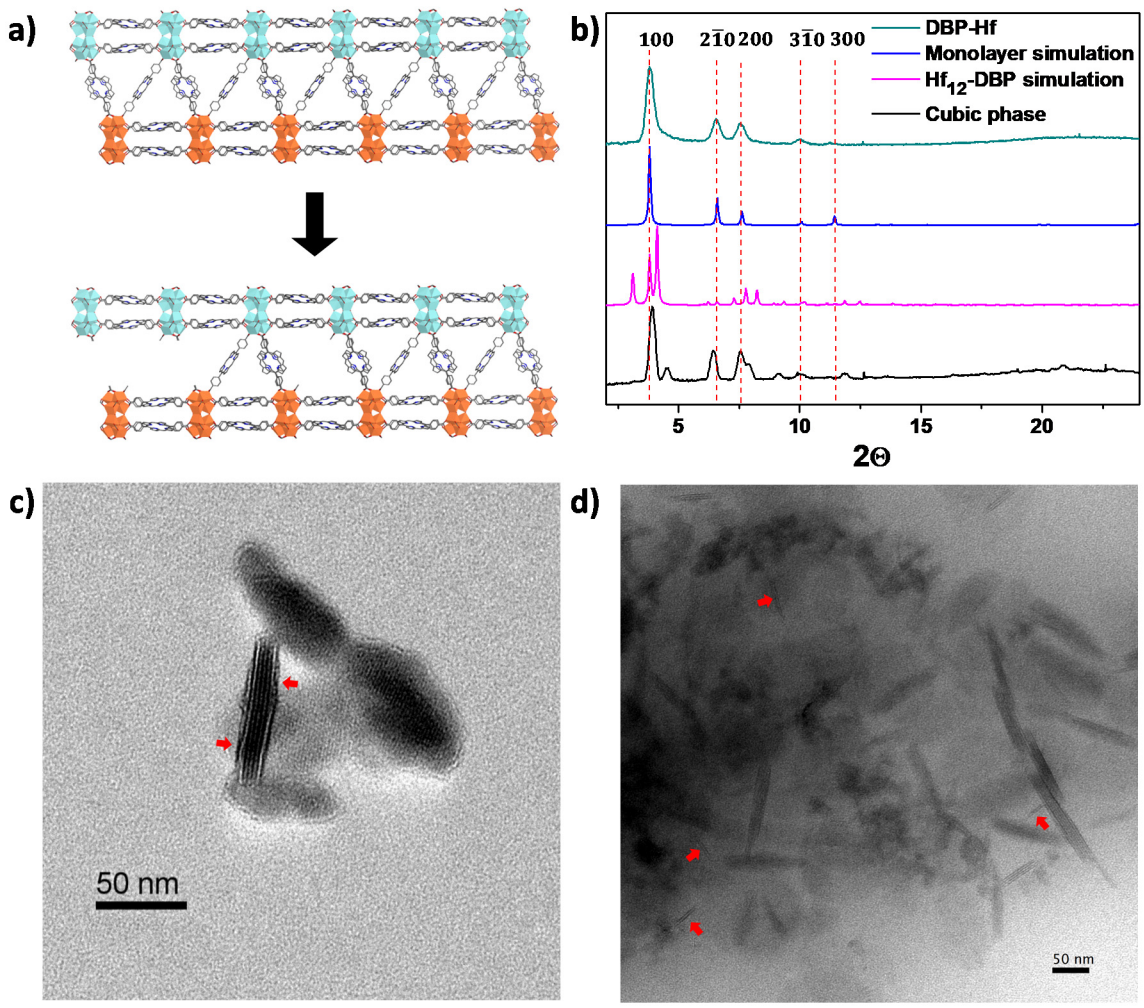

Supplementary Figure 5: Additional structural characterization of DBP-Hf. (a) Schematic illustration of the defects between layers in DBP-Hf. (b) DBP-Hf powder X-ray diffraction pattern compared with those of the cubic (UiO) phase, idealized Hf_{12}-DBP sample, and single layer Hf_{12}-DBP model. The diffraction indices along with the red dotted droplines are for the peaks in Hf_{12}-DBP structure. One of five repetitions with similar results is shown. (c) TEM image of a "standing" particle showing the fusing of layers. Red arrows label the defects of fusing layers in DBP-Hf. (d) A TEM image showing the double layer pieces (red arrows). Three-, four- or multiple layer pieces are also observed in the same sight of view. The TEM images were obtained without repetition.

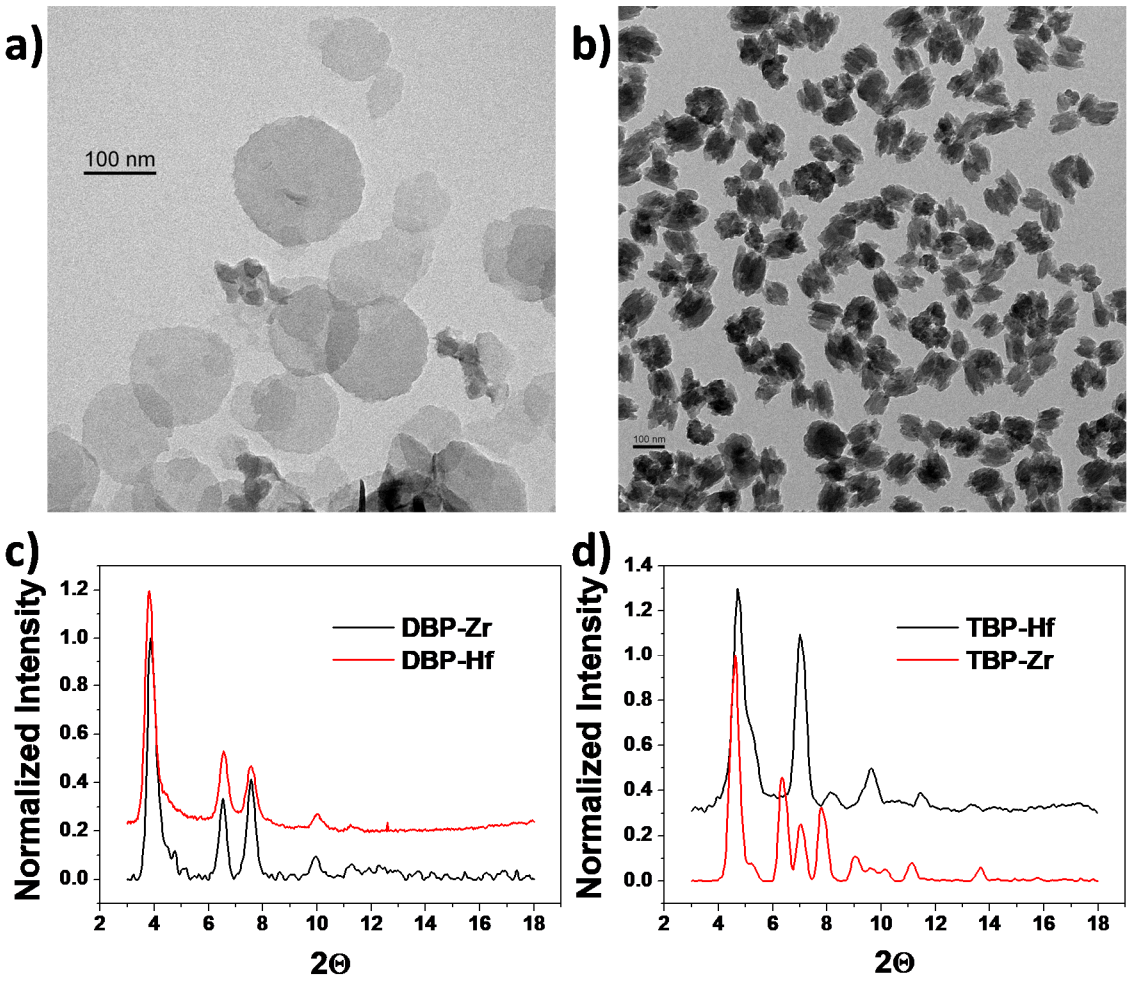

Supplementary Figure 6: TEM images and PXRD patterns of DBP-Zr and TBP-Zr. TEM images of DBP-Zr (**a**) and TBP-Zr (**b**). PXRD patterns of DBP-Zr and DBP-Hf (**c**), TBP-Zr and TBP-Hf (**d**). One of three repetitions with similar results is shown for all the figures.

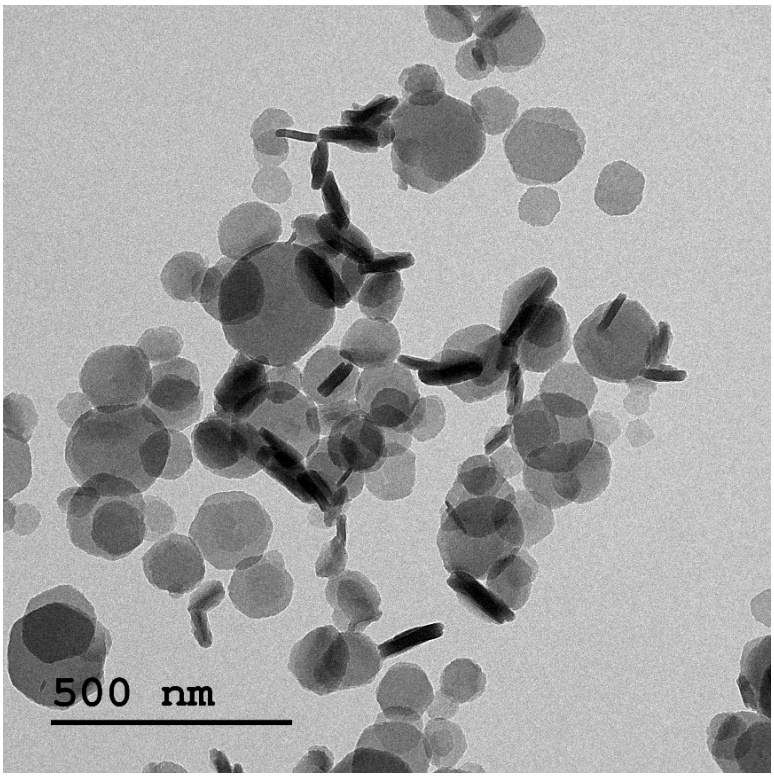

Supplementary Figure 7: TEM image of DBA-Hf. One of over ten repetitions with similar results is shown.

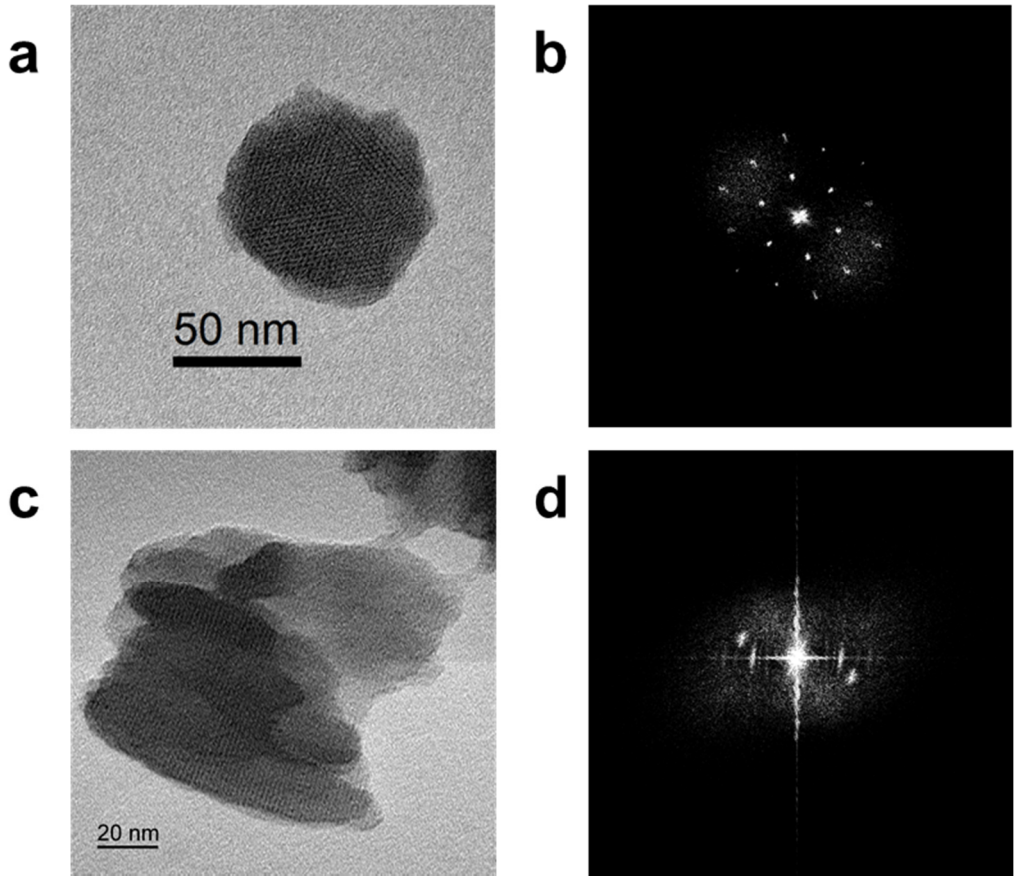

Supplementary Figure 8: High-resolution TEM images of DBP-Hf and TBP-Hf. High-resolution TEM image (a) and fast Fourier transform pattern (b) of DBP-Hf. High-resolution TEM image (c) and fast Fourier transform pattern (d) of TBP-Hf. One of over ten repetitions with similar results is shown.

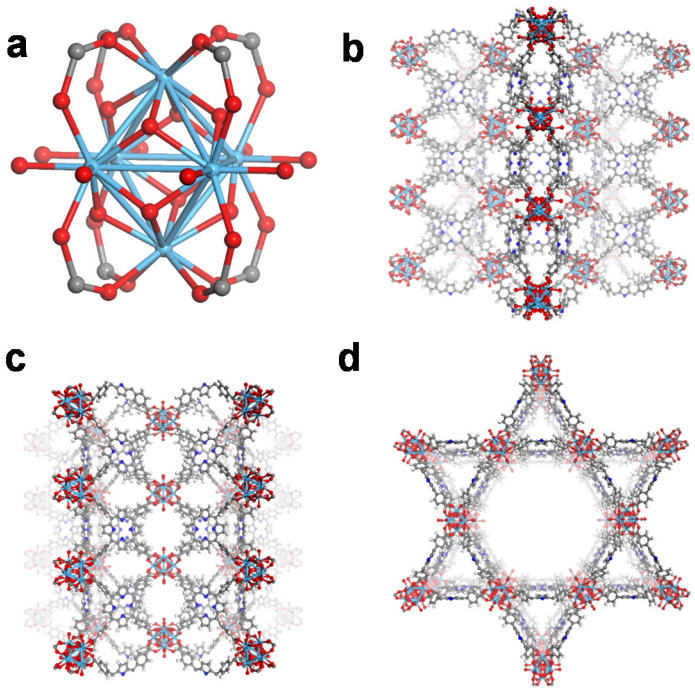

Supplementary Figure 9: Structure figures of TBP-Hf. Ball-and-stick model of SBU $Hf_6(\mu_3\text{-}O)_4(\mu_3\text{-}OH)_4(OH)_4(H_2O)_4(RCO_2)_8$ (RCO_2 is part of the TBP ligand) (a). Ball-and-stick models of TBP-Hf as viewed along the [100] (b), [010] (c) and [001] (d) directions.

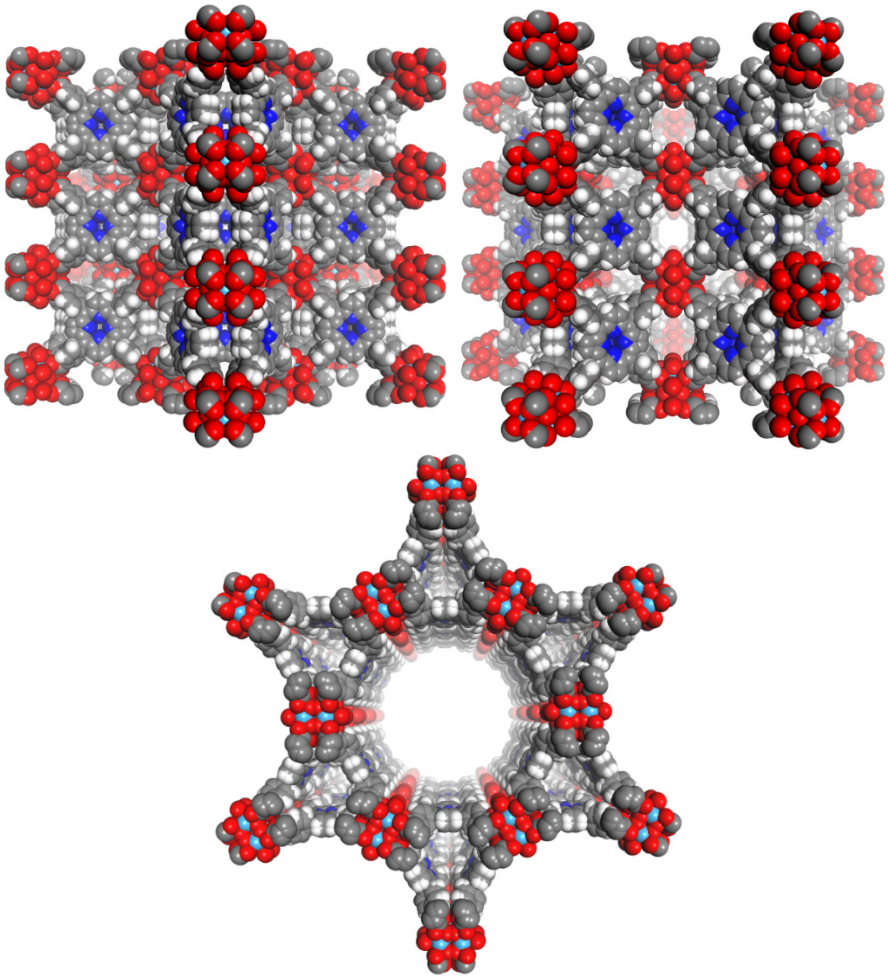

Supplementary Figure 10: Space-filling models of TBP-Hf. The structure was viewed along the [100] (top left), [010] (top right), and [001] (bottom) directions.

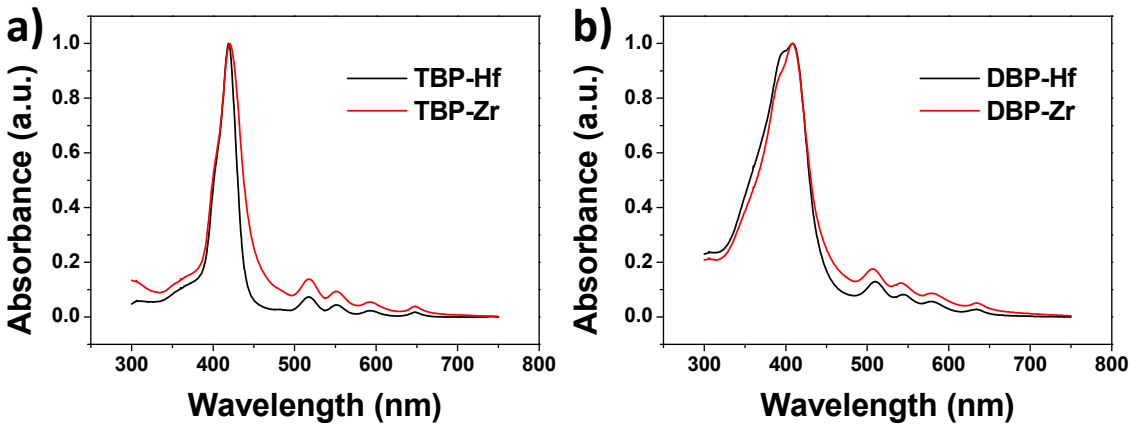

Supplementary Figure 11: UV-vis spectra of Zr and Hf nMOFs. UV-vis spectra of TBP-Zr and TBP-Hf (**a**), DBP-Zr and DBP-Hf (**b**). One of over ten repetitions with similar results is shown for TBP-Hf and DBP-Hf. One of two repetitions with similar results is shown for TBP-Zr and DBP-Zr.

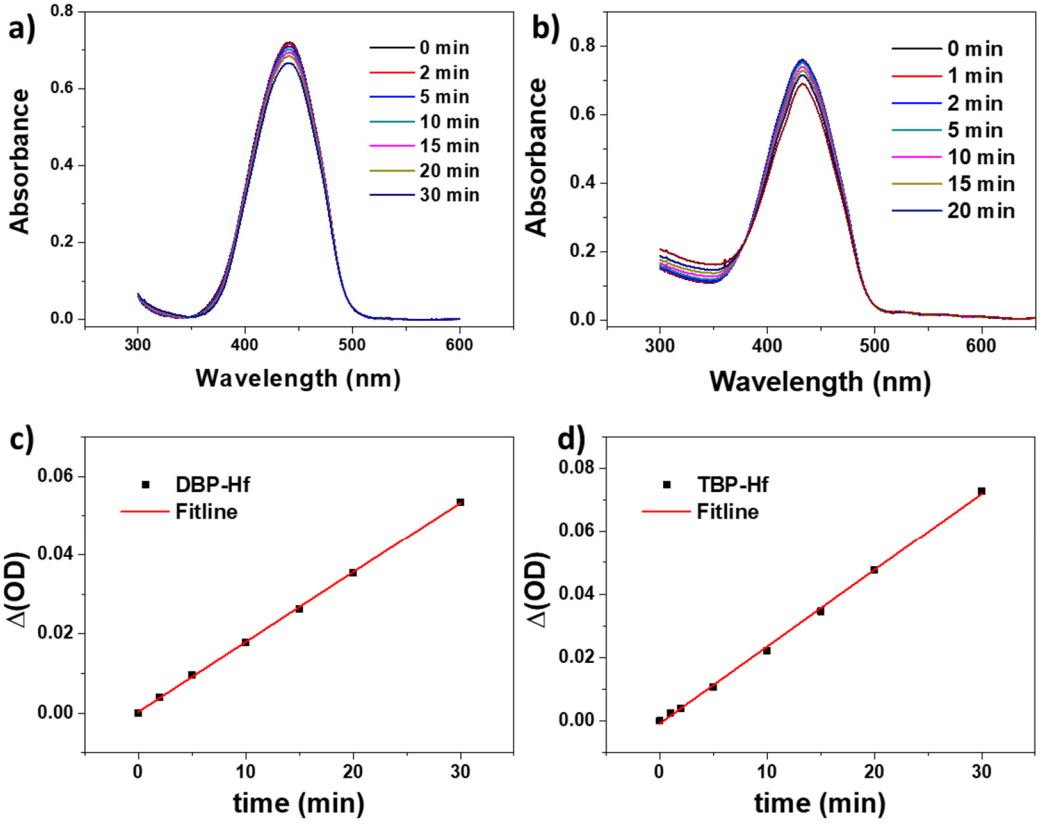

Supplementary Figure 12: Singlet oxygen generation of DBP-Hf and TBP-Hf upon light irradiation. $^1O_2$ generation of DBP-Hf (left) and TBP-Hf (right) upon LED light irradiation (630 nm for DBP-Hf and 650 nm for TBP-Hf, both at 100 mW/cm^2). Linear fit of Δ(OD) against irradiation dose at 439 nm. One of two repetitions with similar results is shown for DBP-Hf. TBP-Hf data was obtained without repetition.

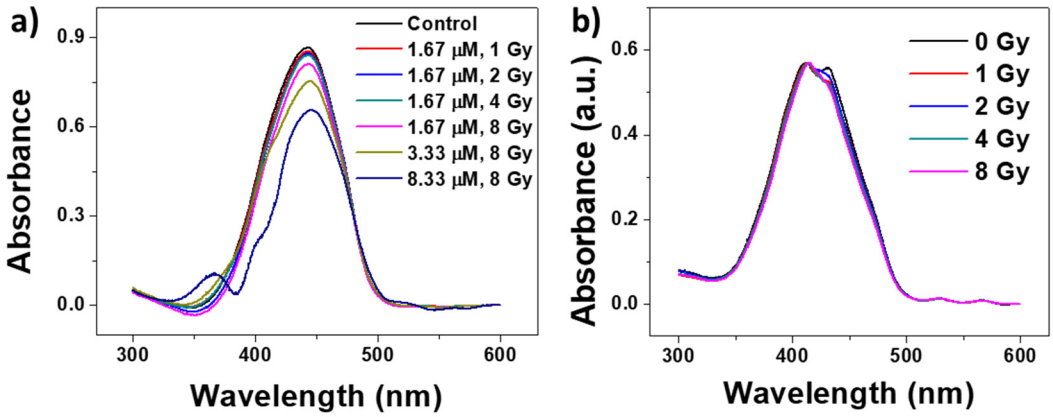

Supplementary Figure 13: Singlet oxygen generation of DBP-Hf and TBP-Hf upon X-ray irradiation. $^1O_2$ of DBP-Hf (a) and TBP-Hf (b) upon X-ray irradiation (225 kVp, 13 mA), indicated by RNO absorption. One of two repetitions for DBP-Hf, 0.83 μM, 8Gy sample and TBP-Hf, 8 Gy sample with similar results were shown. The other groups were acquired without repetition.

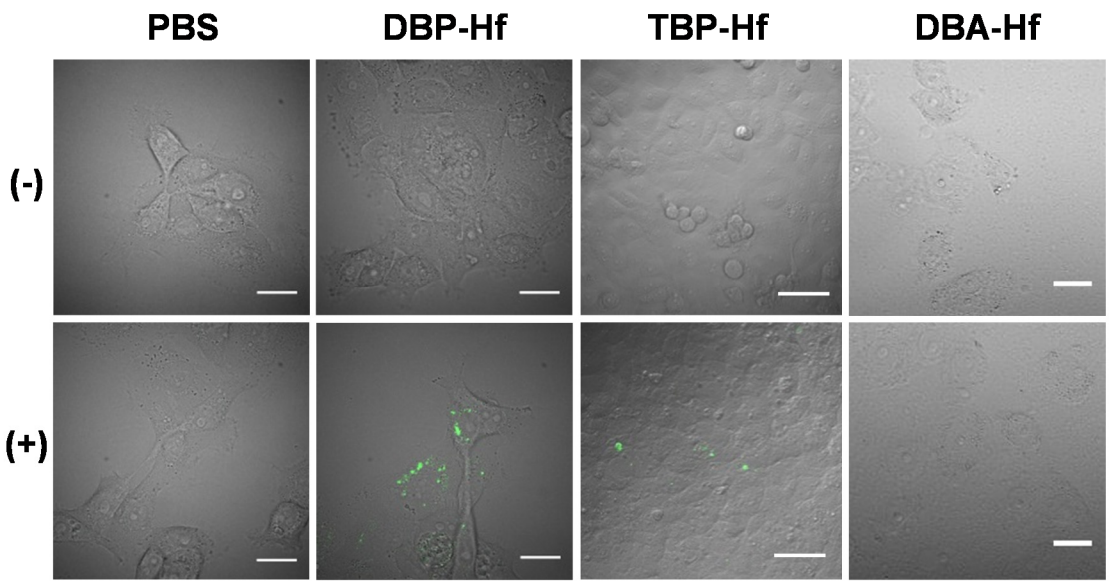

Supplementary Figure 14: Intracellular $^1O_2$ generation detected by SOSG. SQ20B cells were preloaded with SOSG, incubated with PBS, DBP-Hf, TBP-Hf, or DBA-Hf and irradiated at 1 Gy. Green fluorescence from SOSG captured $^1O_2$. Bar=20 μm. (-) and (+) represent dark or 1 Gy irradiation, respectively. The confocal images were obtained without repetition.

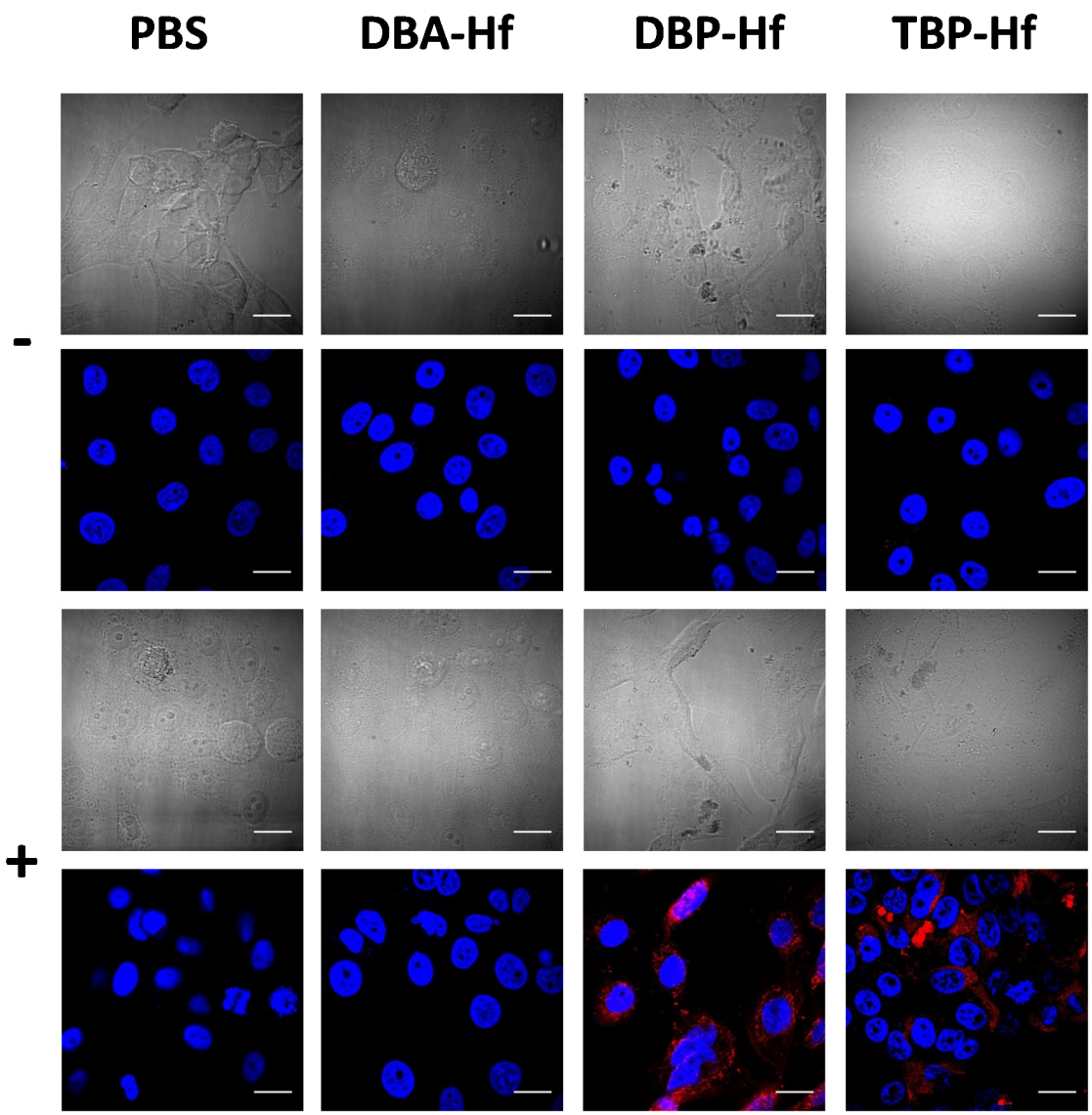

Supplementary Figure 15: COX-2 upregulation detected by Cy3-labeled anti-COX-2 antibody. SQ20B cells were incubated with PBS, DBA-Hf, DBP-Hf, or TBP-Hf, irradiated at 1 Gy, then incubated with biotin-conjugated anti-COX-2 antibody and Cy3-conjugated streptavidin in sequence. Bar=20 μm. (-) and (+) represent dark or 1 Gy irradiation, respectively. The confocal images were obtained without repetition.

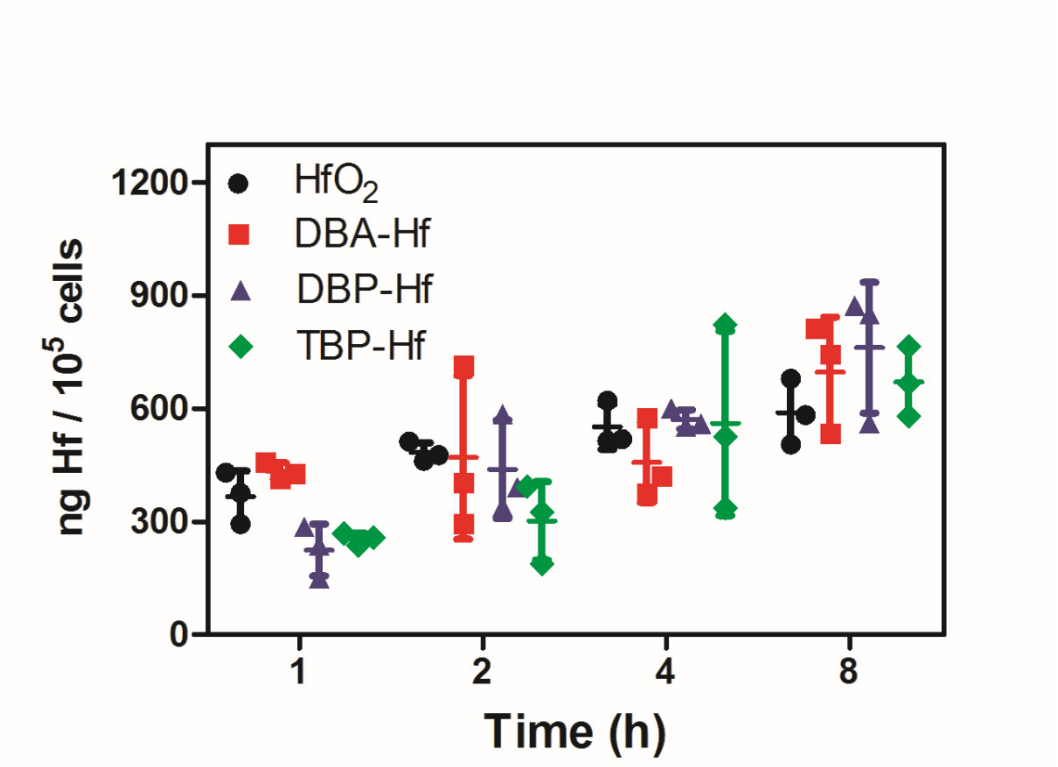

Supplementary Figure 16: Cellular uptake amounts of DBP-Hf, TBP-Hf, DBA-Hf, and HfO_2 nanoparticles in SQ20B cells at different incubation time. The Hf concentrations were determined by ICP-MS. N=3 biologically independent samples for each group. Center values and error bars denote mean and SD, respectively.

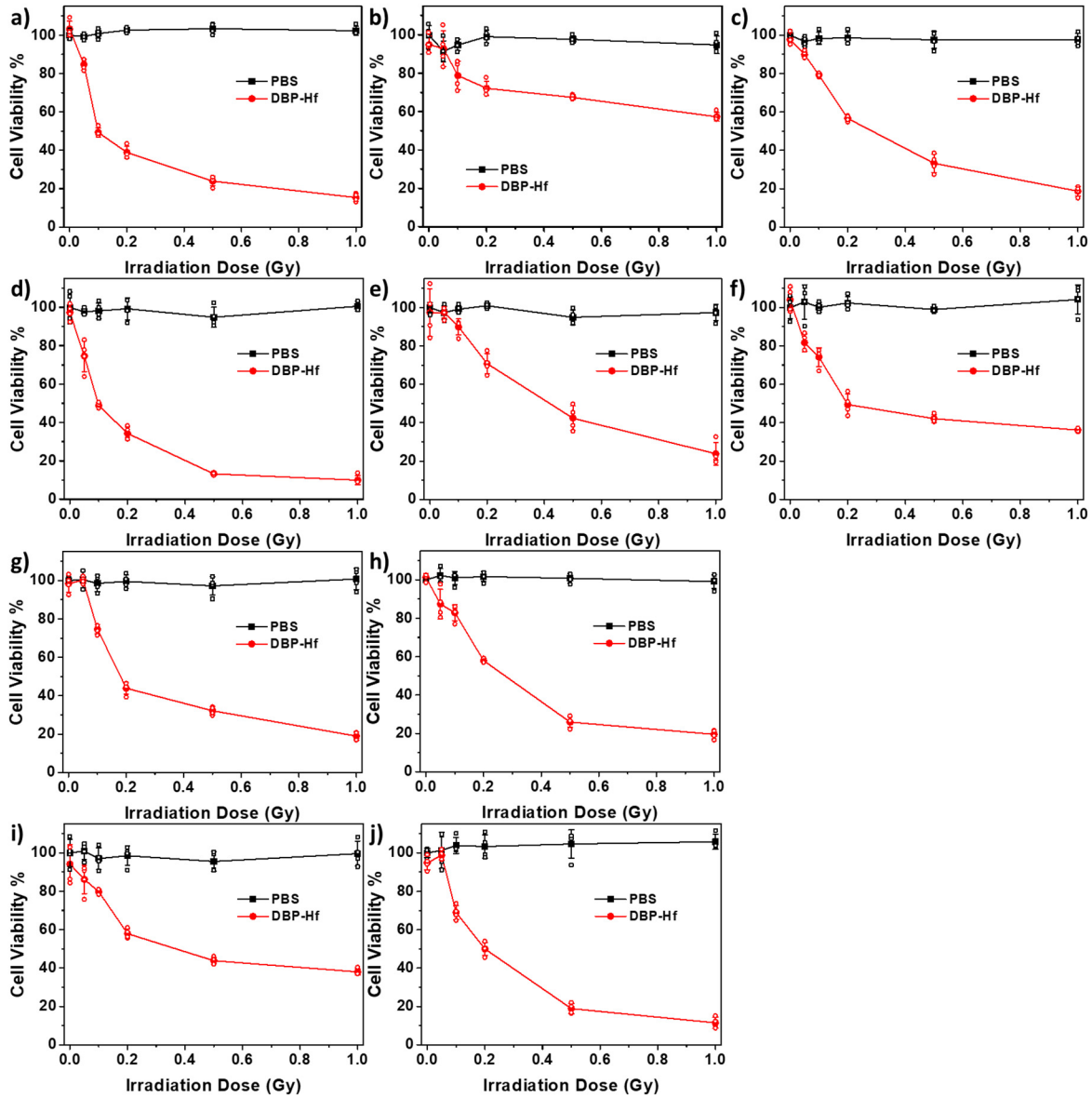

Supplementary Figure 17: Cytotoxicity of DBP-Hf upon X-ray irradiation. Cytotoxicity of DBP-Hf against A2780-cis (**a**), BxPC-3 (**b**), HNSCC135 (**c**), HT29 (**d**), JSQ3 (**e**), MCF-7 (**f**), SCC61 (**g**), SQ20B (**h**), U251 (**i**), and U87 (**j**) cells. The nMOFs were incubated with the cells at a dose of 0.83 μM for 4 h followed by X-ray irradiation at different doses. The cell viability was evaluated by MTS after 72 h. N=4 biologically independent samples for each group. Center values and error bars denote mean and SD, respectively.

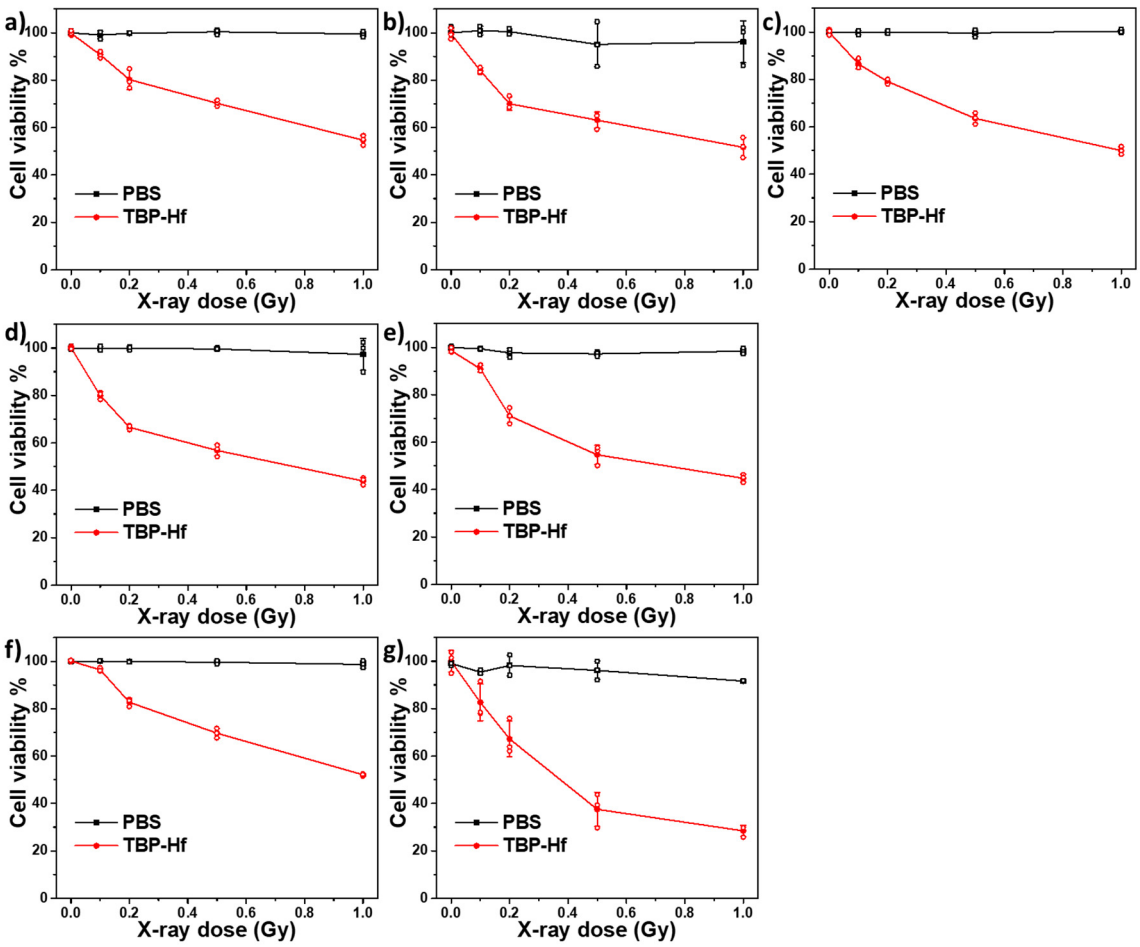

Supplementary Figure 18: Cytotoxicity of TBP-Hf upon X-ray irradiation. Cytotoxicity of TBP-Hf against GL261 (**a**), U251 (**b**), U87 (**c**), CT26 (**d**), TUBO (**e**), TRAMP-C2 (**f**), and SQ20B (**g**) cells. The cells were dosed with 1.67 μM TBP-Hf, and then incubated for 4 h before receiving varying doses of X-ray irradiation. Cell viability was evaluated by MTS after 72 h. N=3 biologically independent samples for each group. Center values and error bars denote mean and SD, respectively.

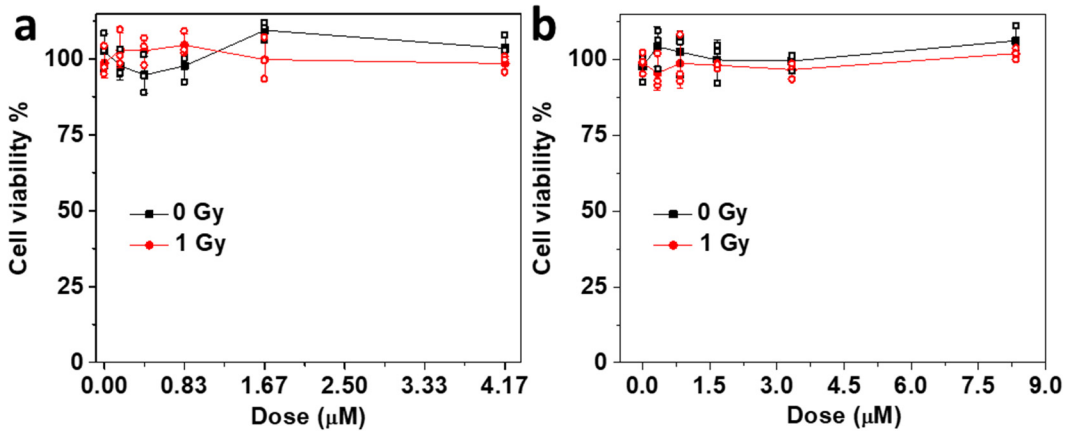

Supplementary Figure 19: Cytotoxicity of DBP-Zr and TBP-Zr upon X-ray irradiation. Cytotoxicity of DBP-Zr (**a**) and TBP-Zr (**b**) against SQ20B cells. Cells were incubated for 4 h with doses of DBP-Zr ranging from 0 to 4.16 μM or TBP-Zr ranging from 0 to 8.33 μM, then irradiated with 1 Gy X-ray. Cells incubated with DBP-Zr or TBP-Zr without X-ray irradiation served as controls. Cell viability was evaluated by MTS after 72 h. N=3 biologically independent samples for each group. Center values and error bars denote mean and SD, respectively.

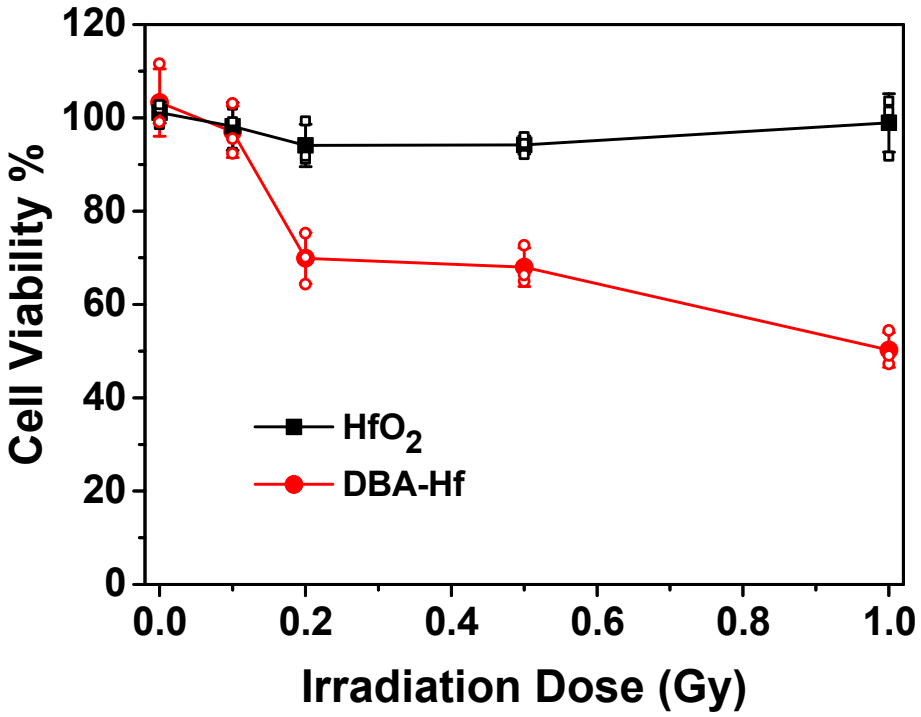

Supplementary Figure S20: Cytotoxicity of DBA-Hf and HfO_2 upon X-ray irradiation against SQ20B cells. DBA-Hf and HfO_2 were incubated with the cells at Hf doses of 10 μM for 4 h followed by X-ray irradiation at different doses. The cell viability was evaluated by MTS after 72 h. N=3 biologically independent samples for each group. Center values and error bars denote mean and SD, respectively.

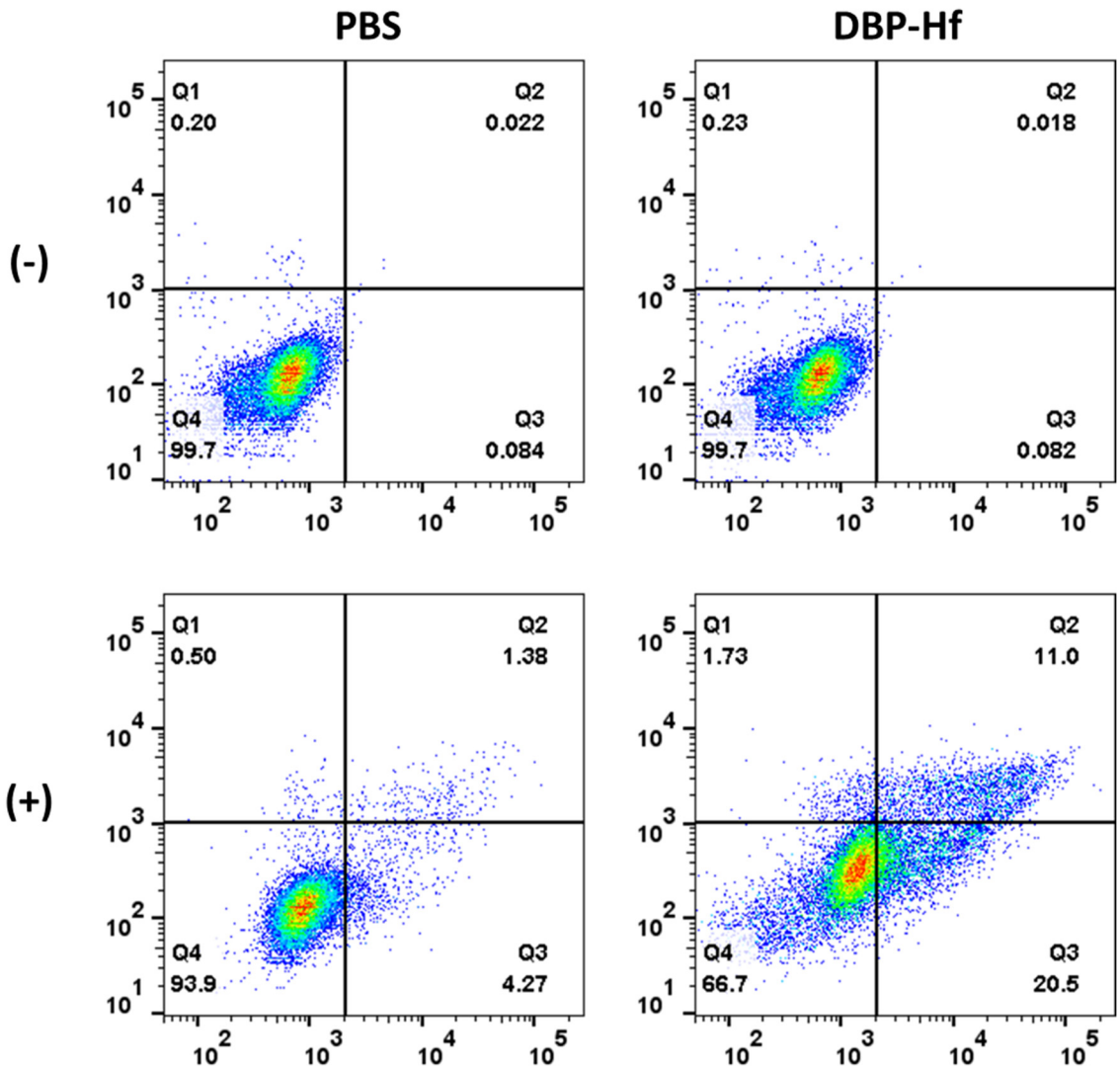

Supplementary Figure 21: Annexin V/PI analysis of CT26 cells incubated with PBS and DBP-Hf with or without X-ray irradiation at a dose of 2 Gy. The quadrants from lower left to upper left (counter clockwise) represent healthy, early apoptotic, late apoptotic, and necrotic cells, respectively. The percentage of cells in each quadrant is shown on the graphs. (+) and (-) refer to with and without irradiation, respectively. One of three repetitions with similar results is shown.

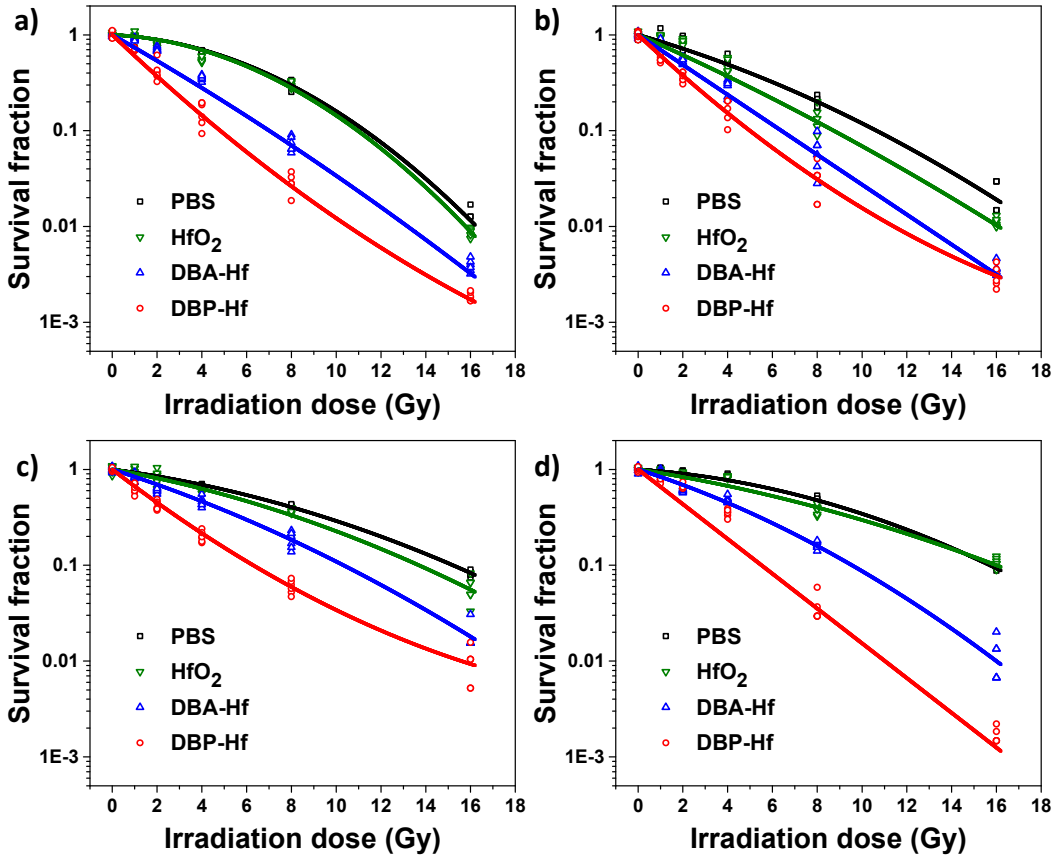

Supplementary Figure 22: Survival curves of DBP-Hf, PBS, HfO_2 and DBA-Hf upon X-ray irradiation. Survival curves of DBP-Hf along with PBS, HfO_2 and DBA-Hf controls upon X-ray irradiation (0-16 Gy doses) on CT26 (a), SQ20B (b), Hela (c), and JSQ3 (d) cell lines by clonogenic assay. The clone counts were converted to survival fractions by normalizing to 0 Gy results in each group. The solid lines are fitted curves with mono- or bi-exponential decay functions. N=6 biologically independent samples for each group. One of two independent experiments with similar results is shown.

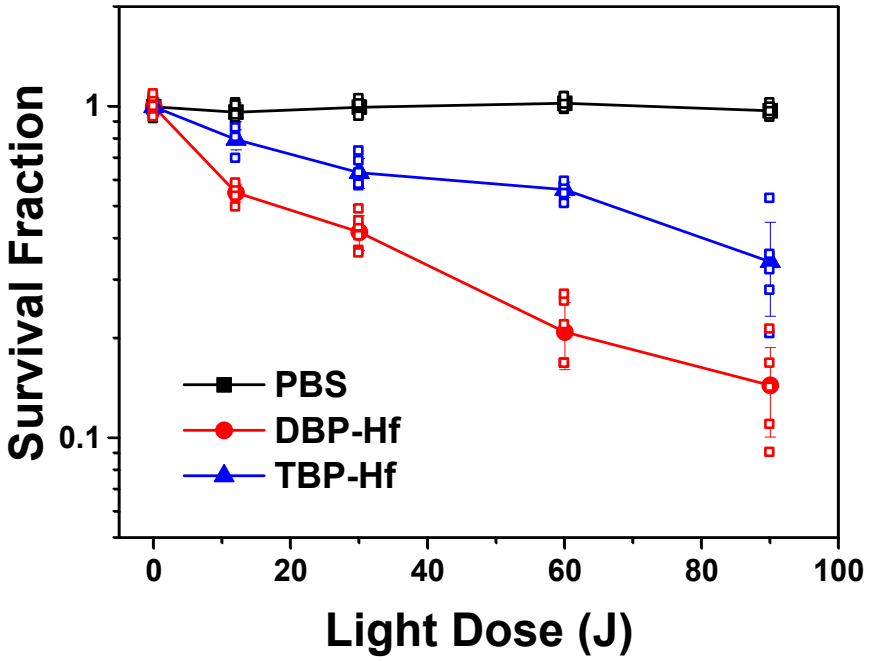

Supplementary Figure 23: Survival curves of PBS, DBP-Hf, or TBP-Hf upon 640 nm LED irradiation on 4T1 cell line by clonogenic assay. The clone counts were converted to survival fractions by normalizing to dark control results in each group. N=6 biologically independent samples for each group. Center values and error bars denote mean and SD, respectively.

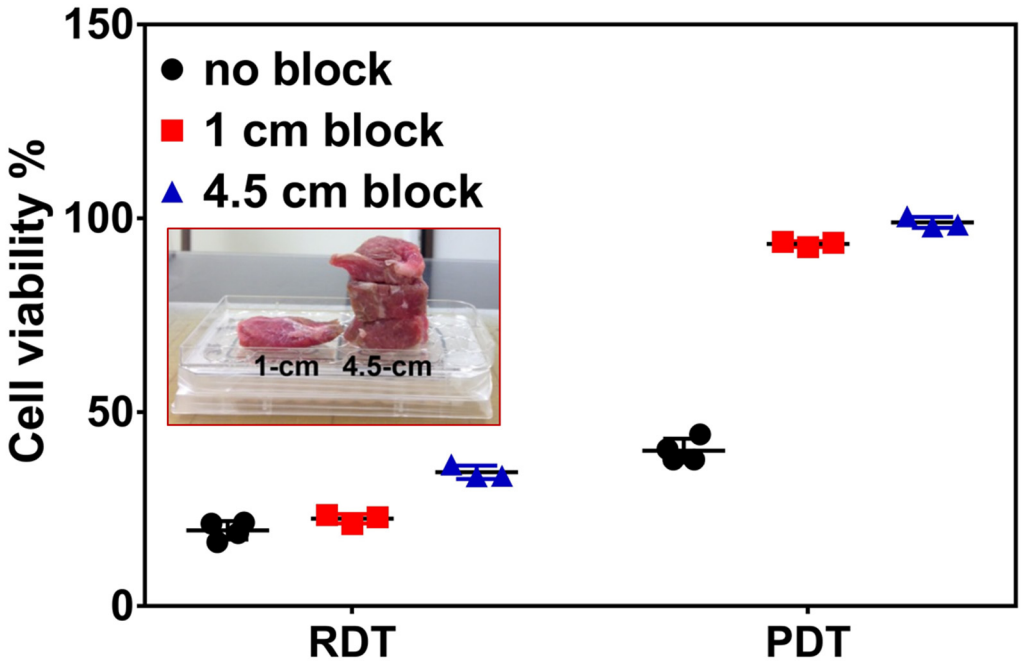

Supplementary Figure 24: Cytotoxicity of SQ20B cells treated with DBP-Hf and X-ray irradiation or LED light irradiation with or without beef as block. N=4 biologically independent samples for no block groups and N=3 biologically independent samples for blocked groups. Center values and error bars denote mean and SD, respectively.

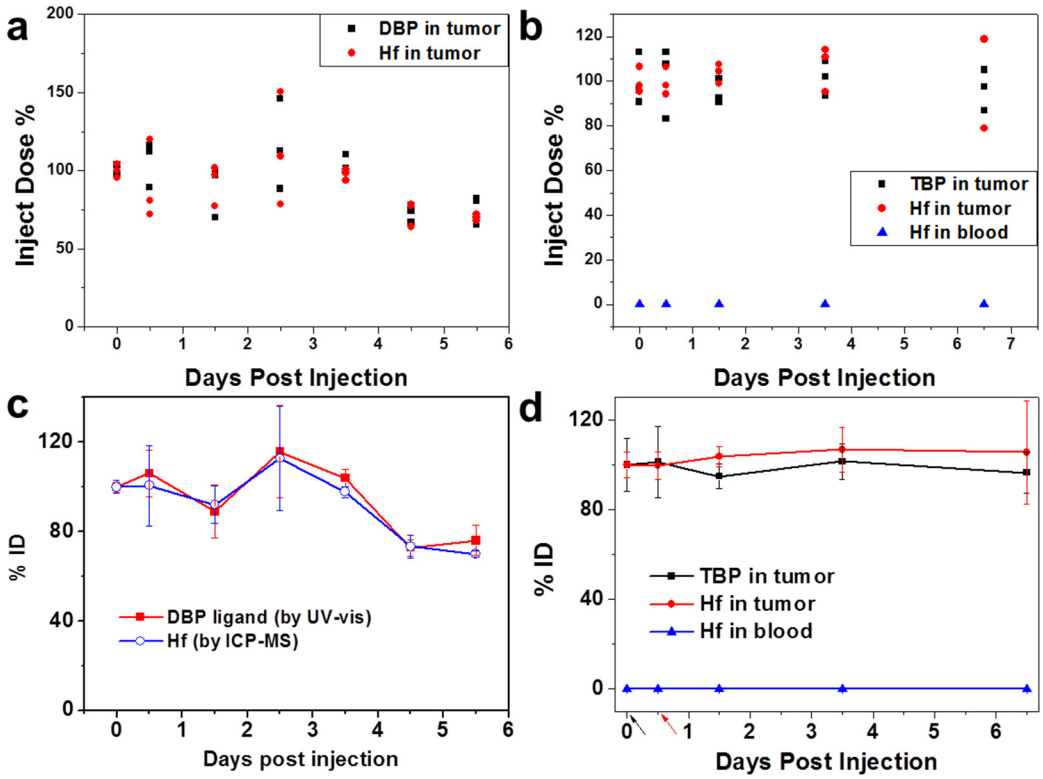

Supplementary Figure 25: Tumour retention of DBP-Hf and TBP-Hf. (**a**) Tumour retention of DBP-Hf in terms of Hf and DBP ligand after intratumoural injection to CT26 tumour-bearing mice. (**b**) Tumour retention and systemic exposure of TBP-Hf after intratumoural injection into CT26 tumour-bearing mice, as measured by ICP-MS (Hf concentration) and UV-vis (TBP concentration). A single dose of 2 Gy X-ray irradiation was given 12 hours after the intratumoural injection of TBP-Hf. Black and red arrows refer to the times TBP-Hf injections and X-ray irradiation were administered. (c) and (d) are the same sets of data plotted in average values and standard deviation. N=3 mice for each group.

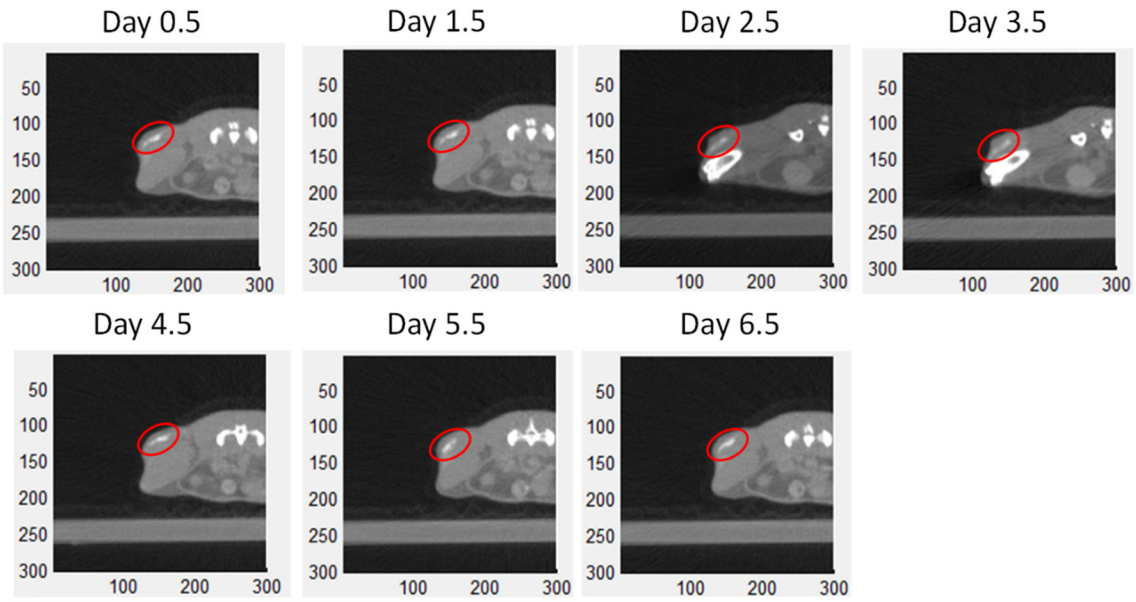

Supplementary Figure 26: CT scan images showing tumour retention of TBP-Hf after intratumoural injection into the CT26 tumour bearing mouse. A single dose of 2 Gy X-ray irradiation was given 12 hours after the intratumoural injection. The red circles highlight the tumour regions with strong contrast of TBP-Hf (white). The images were obtained without repetition.

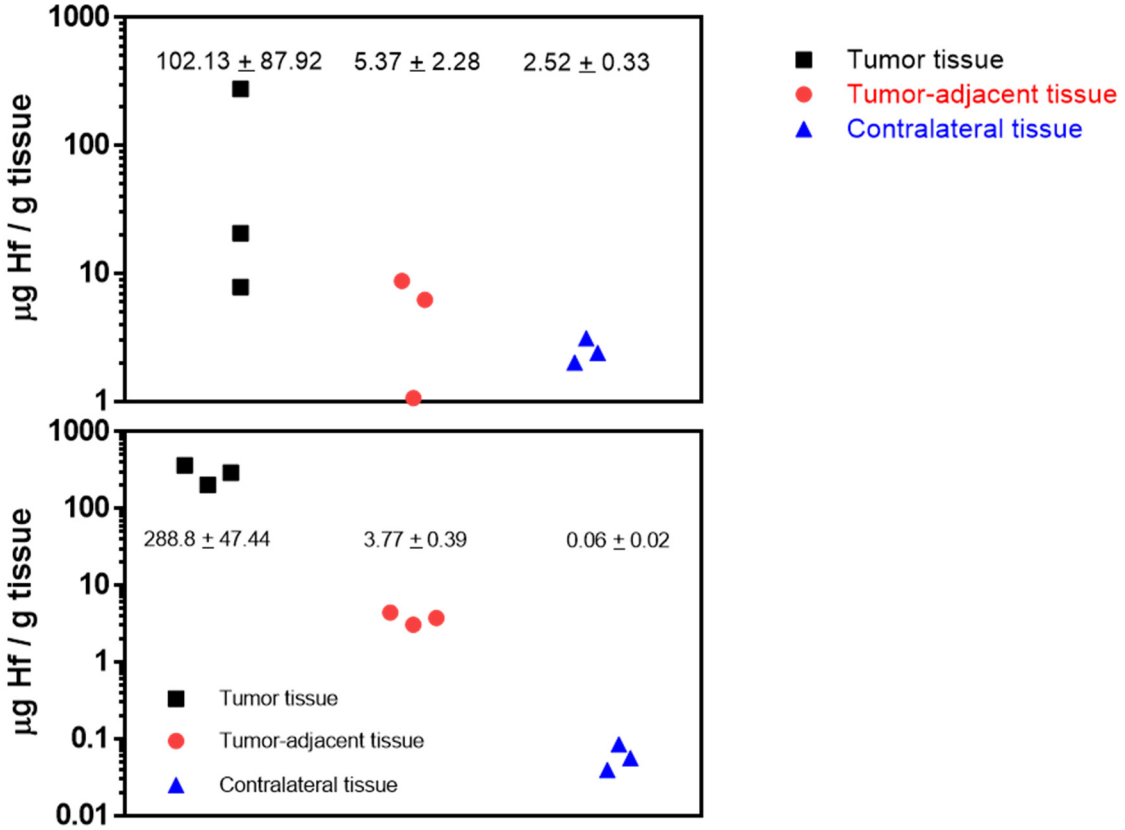

Supplementary Figure 27: Distribution of DBP-Hf and TBP-Hf. Distribution of DBP-Hf (top) and TBP-Hf (bottom) into tumour-adjacent and normal tissues on the contralateral flank after intratumoural injection. The mean ± SEM is shown on the graphs. The concentrations of Hf in the tumour-adjacent and contralateral flank tissue were significantly lower compared to inside the tumour at the end of treatment. The combination of the tumour retention and the highly targeted irradiation beam suggest that there are limited toxicities to tissues outside the tumour. N=3 mice for each group.

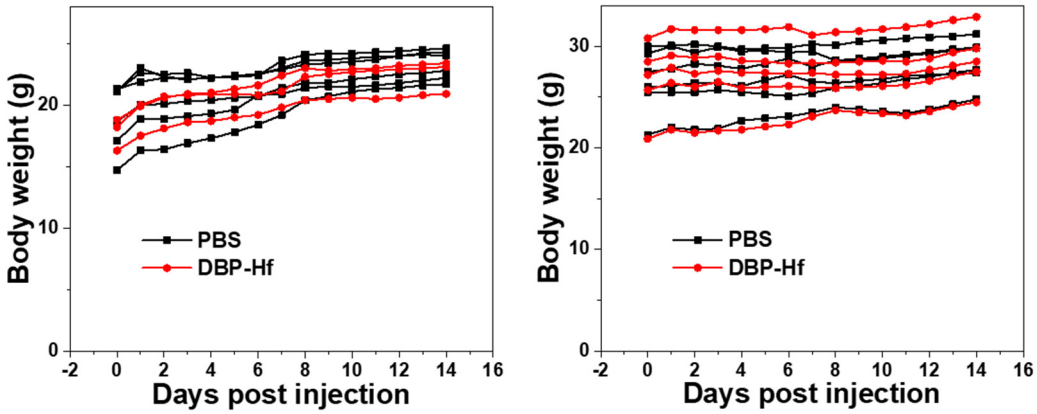

Supplementary Figure 28: Mouse Body Weights. Mean body weights of Balb/c (left) and C57BL/6 (right) mice treated once with 60 mg/kg DBP-Hf or PBS. N=3 mice for Balb/c, DBP-Hf group; N=5 mice for C57BL/6, DBP-Hf group; N=6 mice for PBS groups.

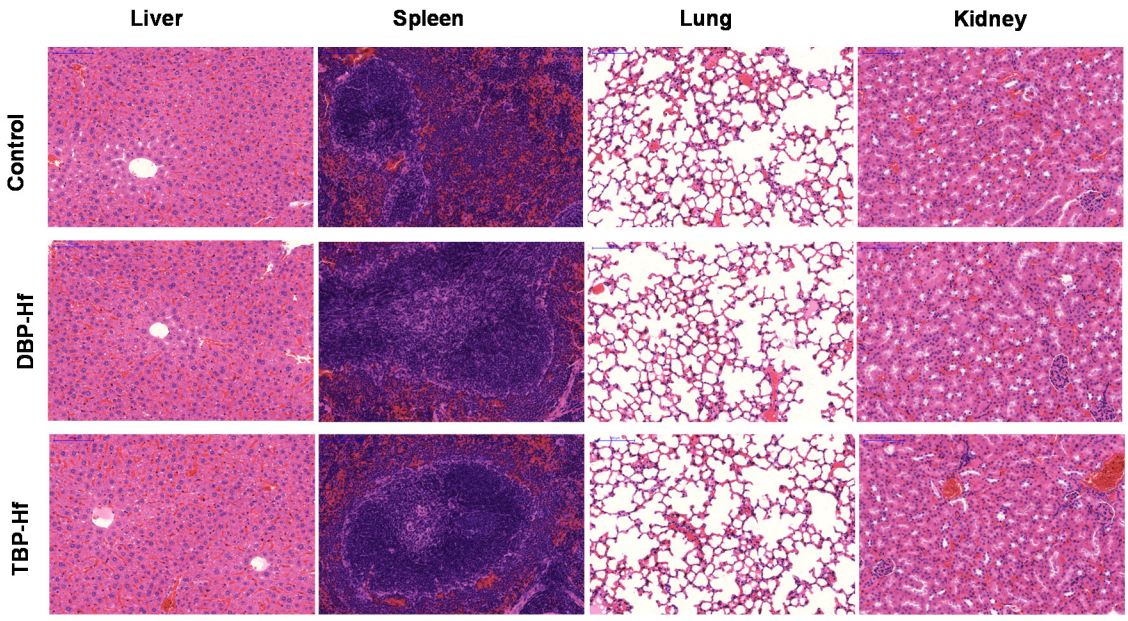

Supplementary Figure 29: Histology of major organs. Histology of frozen sections of major organs of SQ20B tumour bearing mice receiving intratumoural injection of DBP-Hf or TBP-Hf and X-ray irradiation treatment after H&E staining. The data was obtained without repetition.

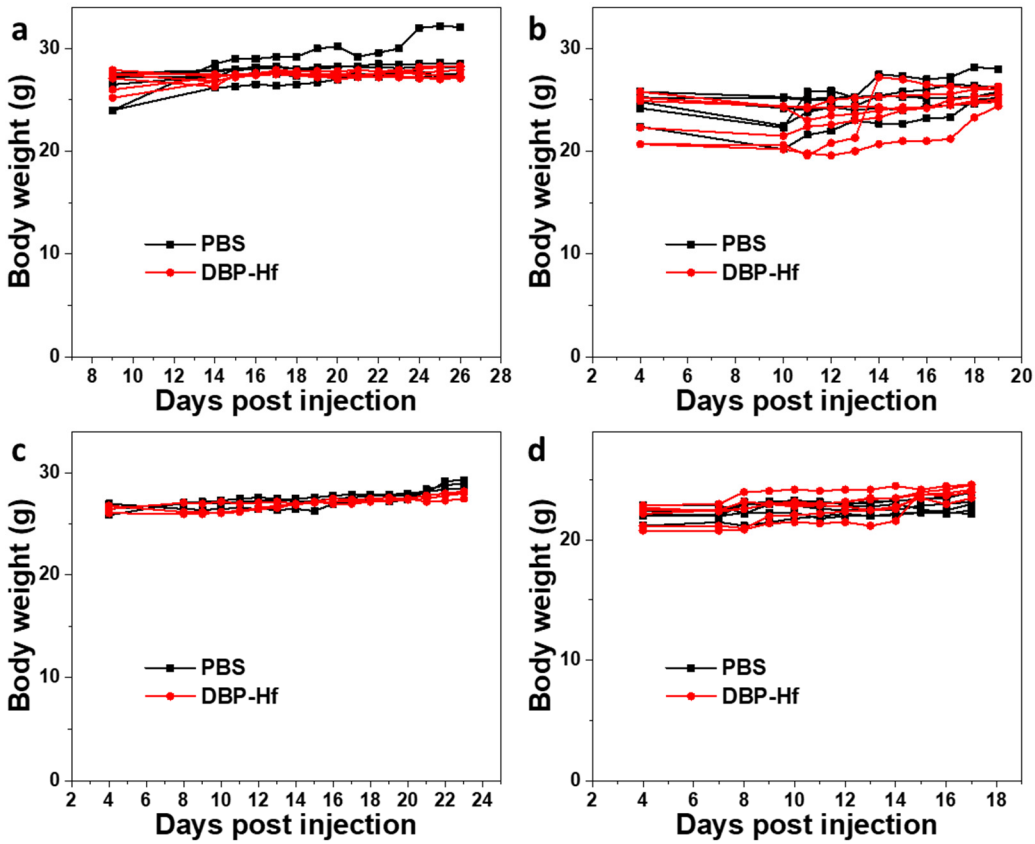

Supplementary Figure 30: Body weights of tumour-bearing mice treated with PBS or DBP-Hf (0.11 mg) in conjunction with X-ray irradiation. Treatments began when tumours reached 100-150 mm^3 in volume. X-ray irradiation was dosed at 0.5 Gy/fraction beginning 12 h after intratumoural injection of PBS or nMOFs for a single dose on U87MG (**a**), or for three consecutive days on SQ20B (**b**), PC-3 (**c**), or CT26 (**d**). N=6 mice in each group for U87MG, SQ20B and CT26 models. N=3 mice in each group for PC-3 model.

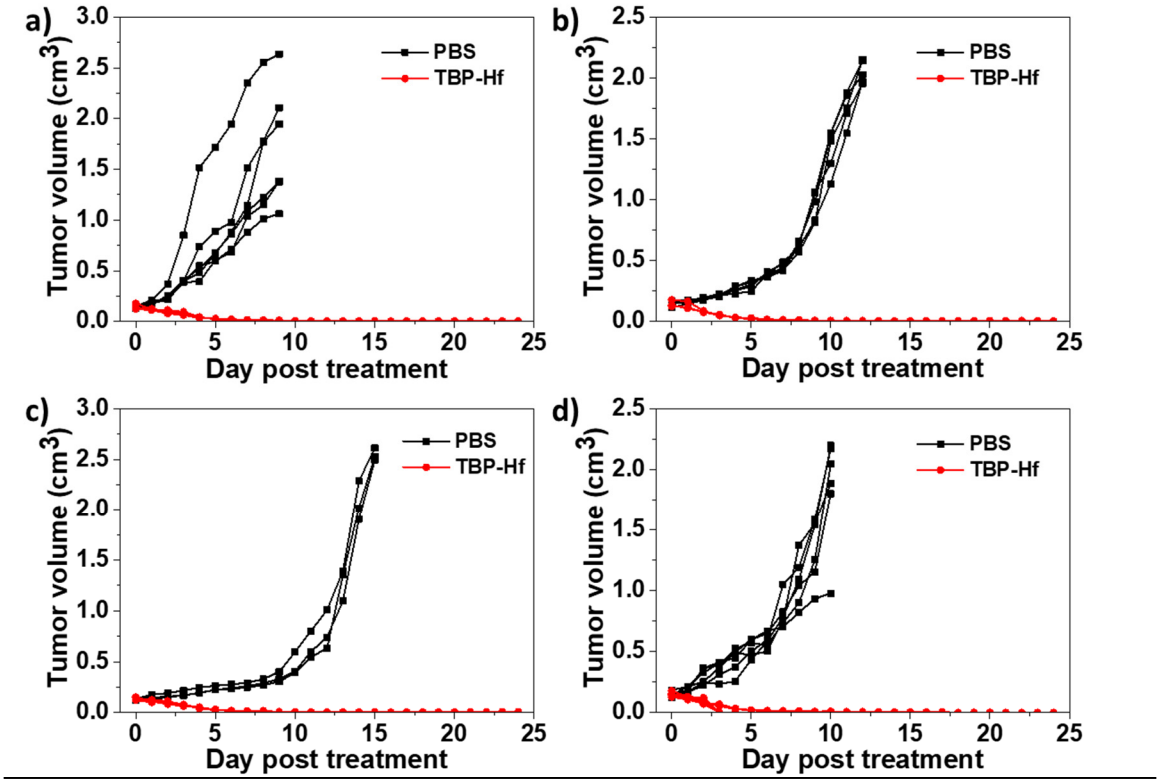

Supplementary Figure 31: Tumour growth curves. Tumour growth curves of head and neck cancer SQ20B (**a**), glioblastoma U87MG (**b**), prostate cancer PC-3 (**c**), or colorectal cancer CT26 (**d**) tumour-bearing mice treated with PBS or TBP-Hf (0.60 mg) in conjunction with X-ray irradiation. Treatments began when tumours reached 100-150 mm^3 in volume. Mice were subjected to X-ray irradiation 12 h after the intratumoural injections of PBS or TBP-Hf on five consecutive days at a dose of 1 Gy/fraction. Black arrows refer to the times of PBS or TBP-Hf injection while red arrows indicate the times of X-ray irradiations. N=6 mice in PBS group for SQ20B and both PBS and TBP-Hf groups for CT26. N=5 mice in PBS group for U87MG. N=3 mice in TBP-Hf groups for SQ20B, U87MG and PC-3, and PBS group for PC-3.

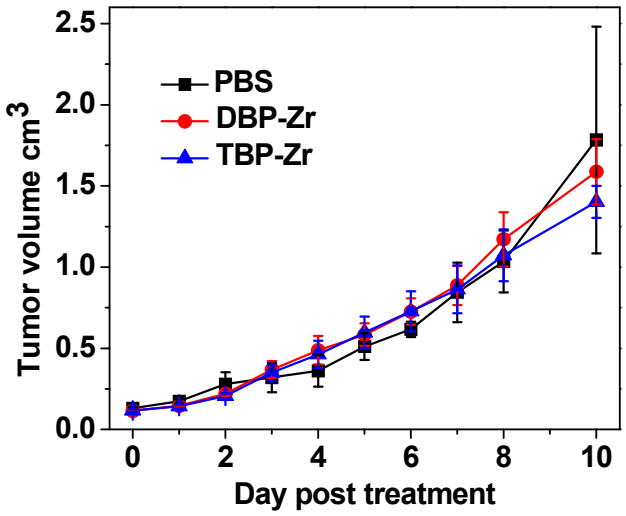

Supplementary Figure 32: Tumour growth curve of murine colorectal cancer CT26 tumour-bearing mice treated with PBS, TBP-Zr (0.48 mg), or DBP-Zr (0.10 mg) and X-ray irradiation. Treatments began when the tumours reached 100-150 mm^3 in volume. The X-ray irradiation was carried out on mice 12 h post the intratumoural injection of PBS or TBP-Zr on five consecutive days at a dose of 1 Gy/fraction. For DBP-Zr, the X-ray irradiation was carried out on mice 12 h post the intratumoural injection of DBP-Zr on 3 consecutive days at a dose of 0.5 Gy/fraction. N=5 mice for each group. Center values and error bars denote mean and SD, respectively.

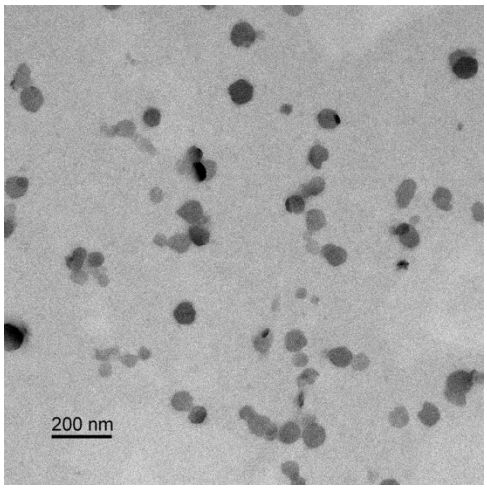

Supplementary Figure 33: TEM image of DBP-Hf@PEG. One of two repetitions with similar results is shown for all the figures.

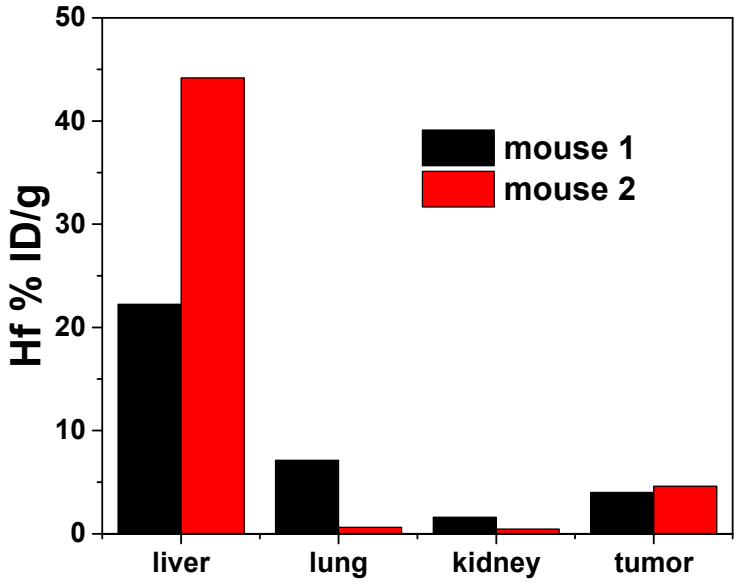

Supplementary Figure 34: Biodistribution of DBP-Hf@PEG 24 h after i.v. injection to CT26 tumour-bearing mice as determined by ICP-MS. N=2 mice.

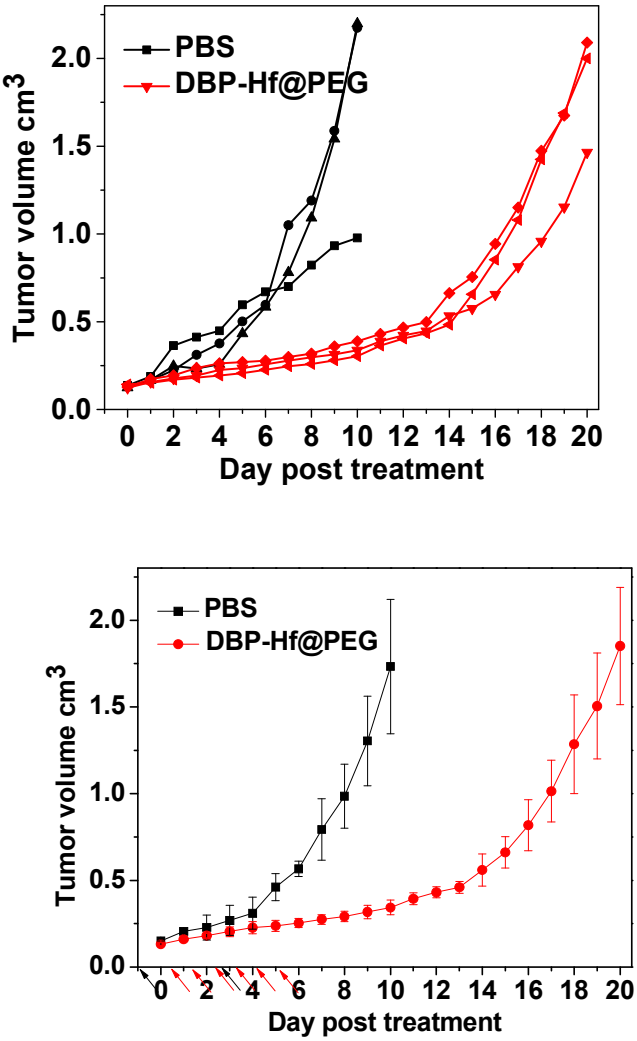

Supplementary Figure 35: Tumour growth curves of DBP-Hf@PEG upon X-ray irradiation (120 kVp, 20 mA, 2-mm Cu filter) on CT26 tumour-bearing mice. Individual data points (top) analyzed data (bottom) are shown. DBP-Hf@PEG was i.v. injected into mice every three days for a total of 2 injections, followed by daily X-ray irradiation at a dose of 1 Gy/fraction, for a total of 6 fractions. Black and red arrows refer to particle injection and X-ray irradiation, respectively. N=3 mice for each group. Center values and error bars denote mean and SD, respectively.

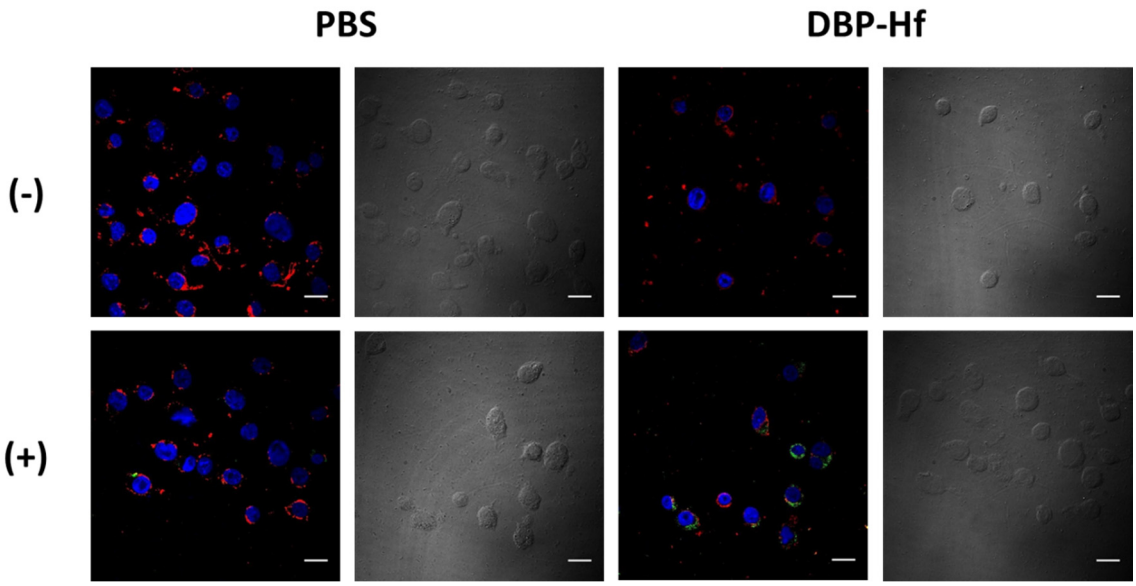

Supplementary Figure 36: Immunofluorescence microscopy of CRT expression on the cell surface of CT26 treated with PBS or DBP-Hf with (+) or without (-) X-ray irradiation. Blue, red and green fluorescence show DAPI-stained nucleus, cell membrane and CRT exposure on the cell surface, respectively. From left to right: fluorescence and bright field image of PBS control and DBP-Hf, respectively. Scale bar = 20 μm. The confocal images were obtained without repetition.

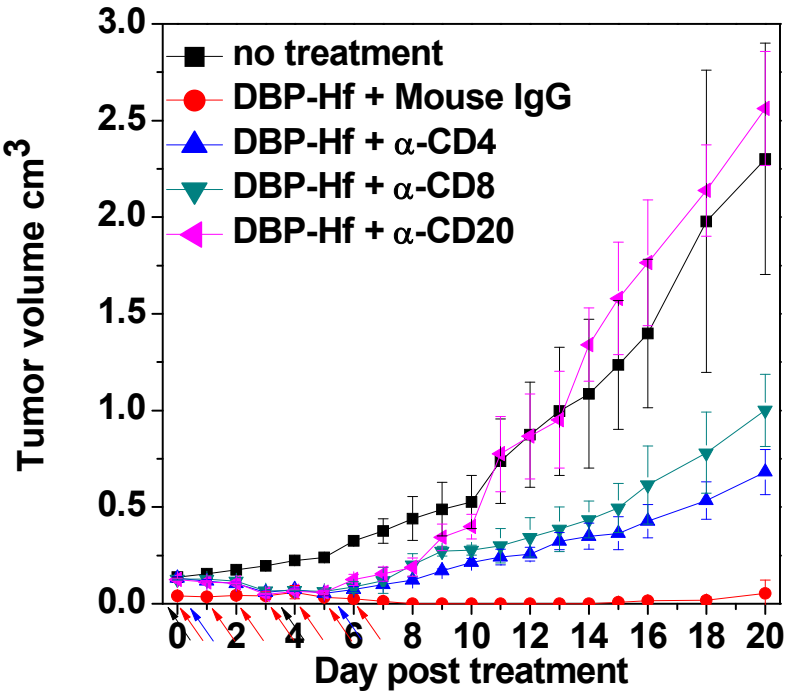

Supplementary Figure 37: Tumour growth curves of TUBO tumour bearing BALB/c mice with T cell or B cell depletion and treated with DBP-Hf (0.11 mg) and X-ray irradiation. Treatments began when the tumours reached 100-150 mm^3 in volume. The X-ray irradiation (0.5 Gy/fraction) was carried out on mice 12 h post intratumoural injection of DBP-Hf on 6 consecutive days. N=3 mice for each group. Centers and error bars denote mean and SD, respectively.

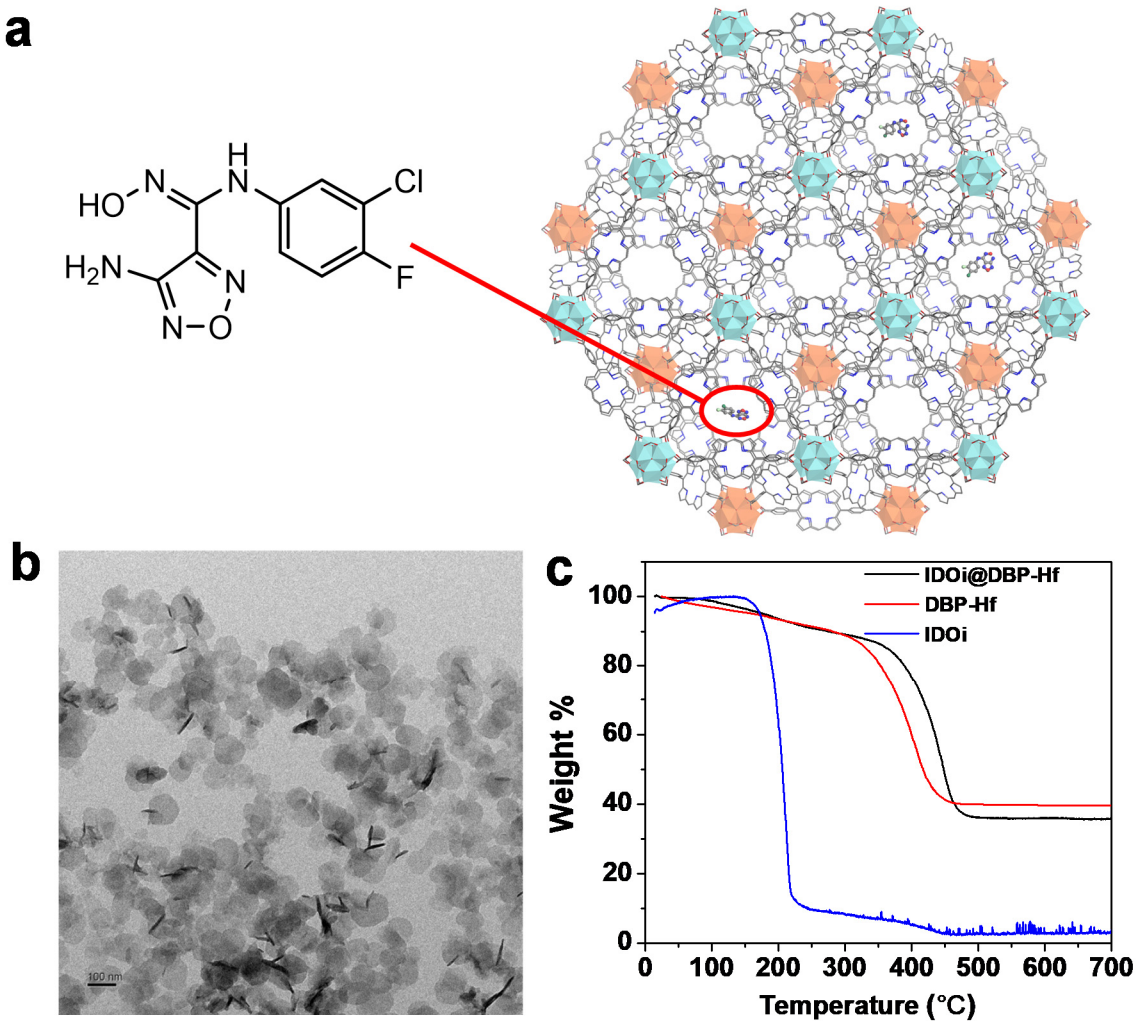

Supplementary Figure 38: Synthesis and characterization of IDOi@DBP-Hf. (**a**) Scheme to show the IDO inhibitor loading to the nMOF. (**b**)TEM and (**c**)TGA of IDOi@DBP-Hf. One of two independent experiments with similar results is shown.

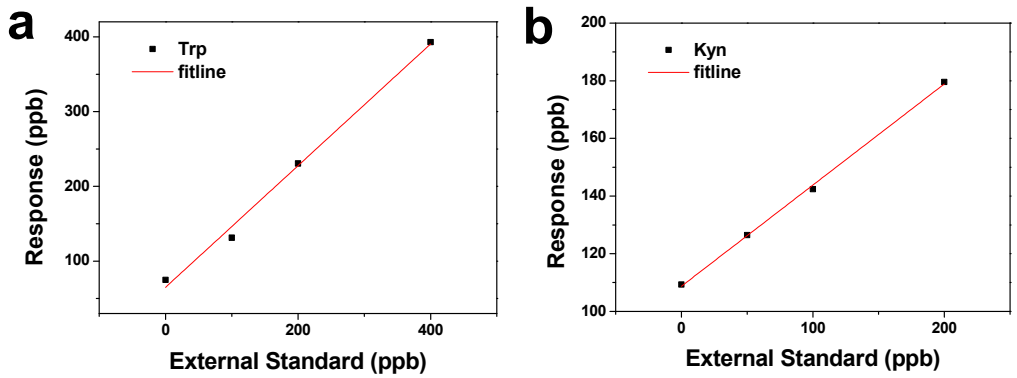

Supplementary Figure 39: Standard curves of tryptophan and kynurenine by LC-MS. Tryptophan (**a**) and kynurenine (**b**).

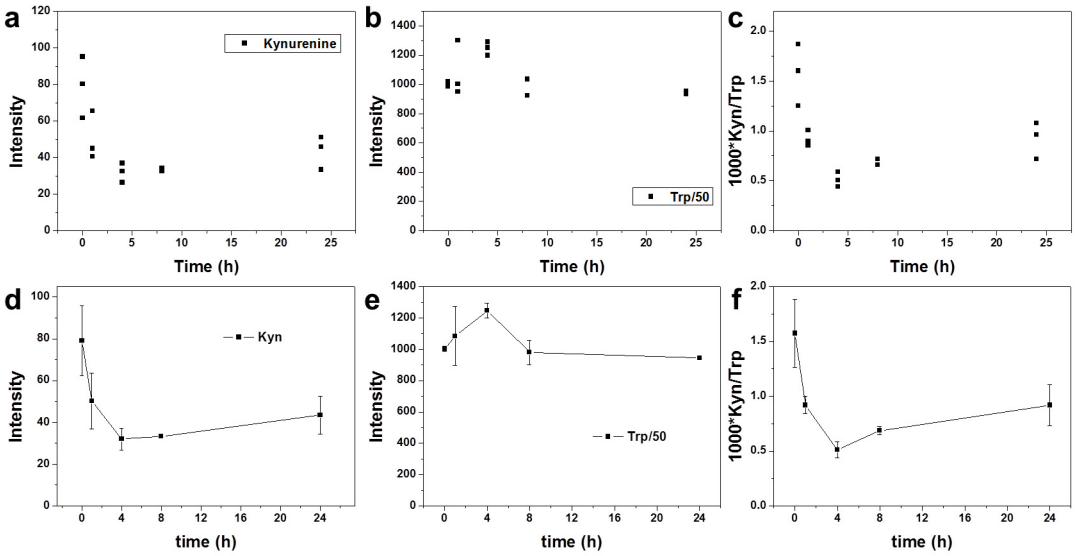

Supplementary Figure 40: Plasma Kyn, Trp, and Kyn/Trp ratios. Plasma Kyn (**a**), Trp (**b**), and Kyn/Trp ratio (**c**) evolutions of mice receiving i.t. injection of IDOi@DBP-Hf at a dose of 0.11 mg DBP-Hf and 0.58 mg/kg IDOi over 24 hours. (d)-(f) are the same sets of data plotted in average values and standard deviation. N=3 mice for each group. The Kyn and Trp concentrations in the plasma were determined by LC-MS.

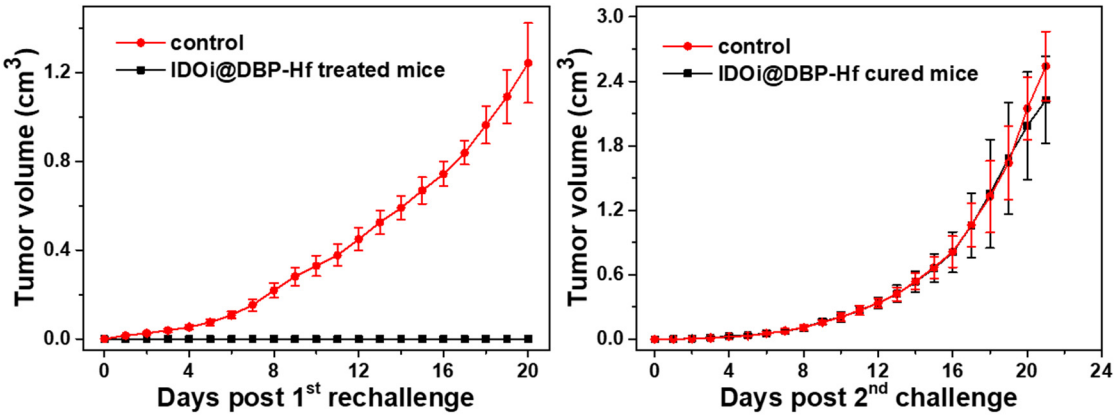

Supplementary Figure 41: Tumour growth curves after the first tumour rechallenge. Tumour growth curves after the first tumour rechallenge with TUBO cells (left) and the second tumour rechallenge with CT26 cells (right). Day 0 of the first and the second rechallenges corresponds to day 37 and day 97 after the first treatment in **Fig 4f**, respectively. N=6 mice for each control group and N=4 mice for the 2nd challenge cured mice group. Centers and error bars denote mean and SD, respectively.

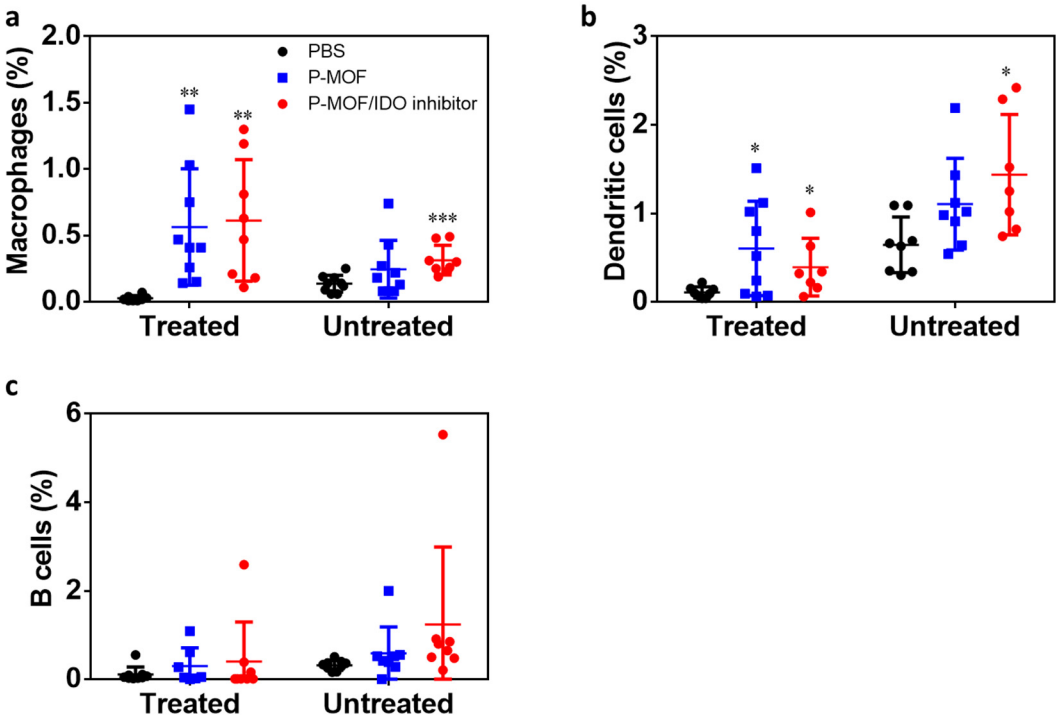

Supplementary Figure 42: Macrophage, dendritic cell, and B cell profiling by flow cytometry. Bilateral tumour models of TUBO were established and treated as described in **Figure 4c-d**. The right and left tumours were collected for flow cytometry analysis. Percentages of tumour-infiltrating macrophages (**a**), dendritic cells (**b**), and B cells (**c**). *P* values were calculated in two-tailed t-test between treatment groups and PBS. *: $P < 0.05$ from control; **: $P < 0.01$ from control; ***: $P < 0.001$ from control. N=9 mice for each group. Centers and error bars denote means and SD, respectively.

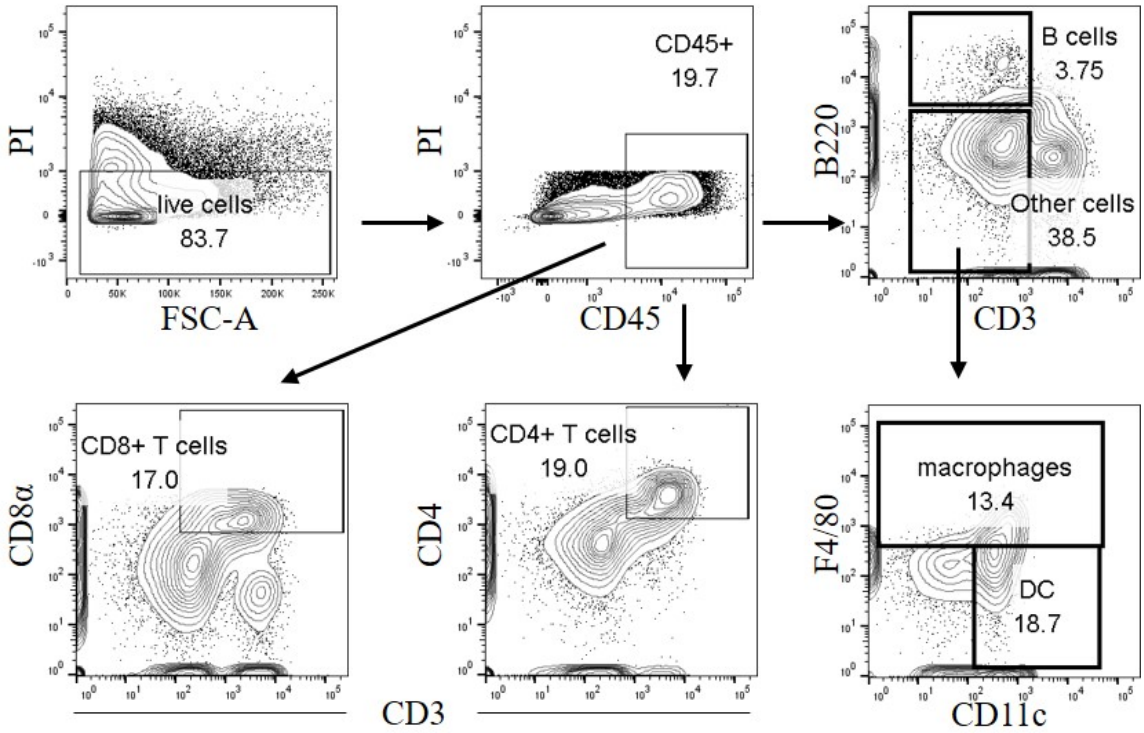

Supplementary Figure 43: Gating strategy of flow cytometry studies. All cells were gated from PI negative cells. Total leukocytes were gated on $CD45^+$ cells; $CD8^+$ T cells were gated on $CD8\alpha^+CD3^+$ $CD45^+$ cells; $CD4^+$ T cells were gated on $CD4^+CD3^+$ $CD45^+$ cells; B cells were gated on $B220^+CD3^-$ $CD45^+$ cells; macrophages were gated on $F4/80^+B220^-CD3^-CD45^+$ cells; dendritic cells were gated on $CD11c^+F4/80^-B220^-CD3^-CD45^+$ cells.

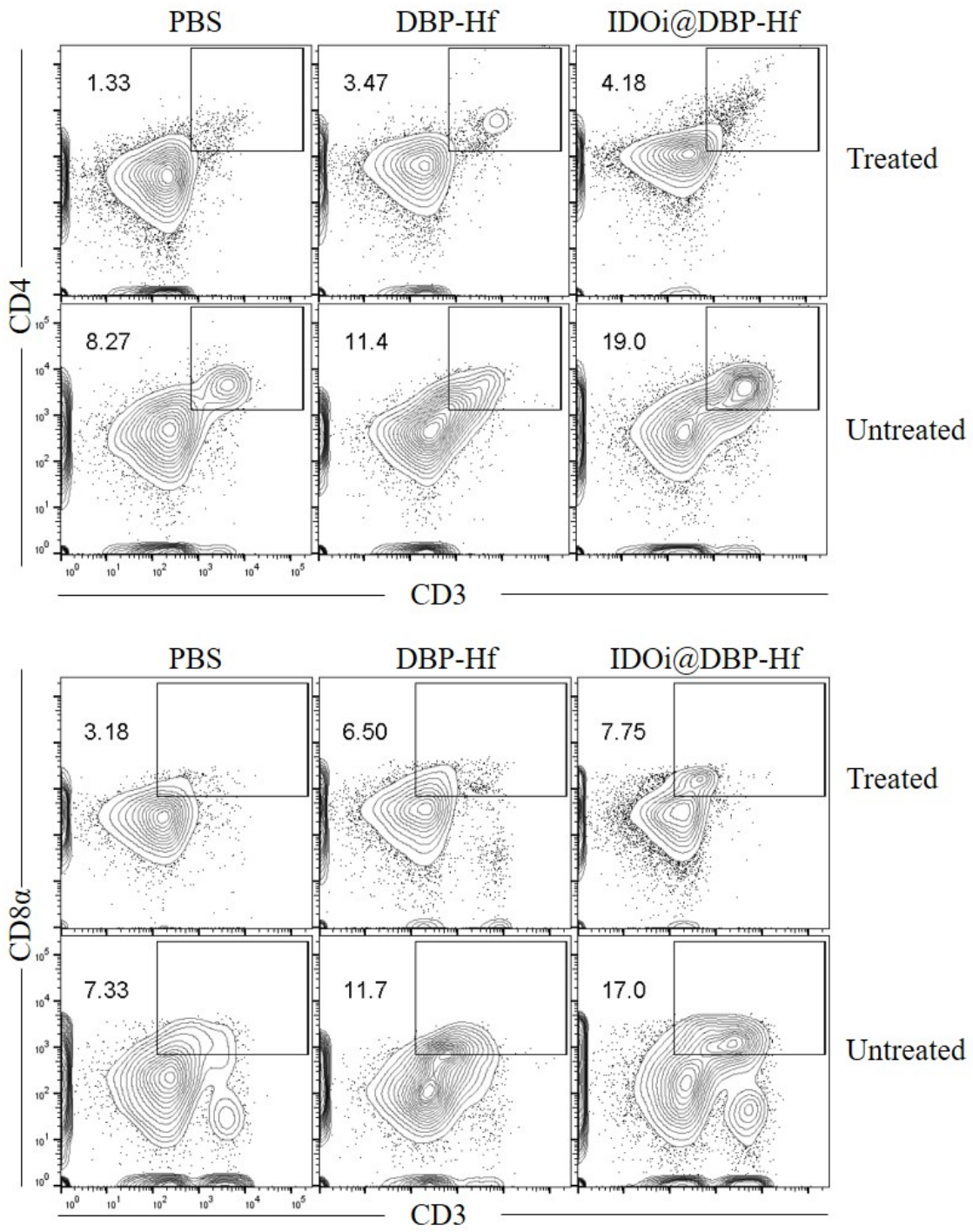

Supplementary Figure 44: Representative flow cytometry plots. Tumour infiltrating $CD4^+$ T cells (top) and $CD8^+$ T cells (bottom). One of two repetitions with similar results is shown.

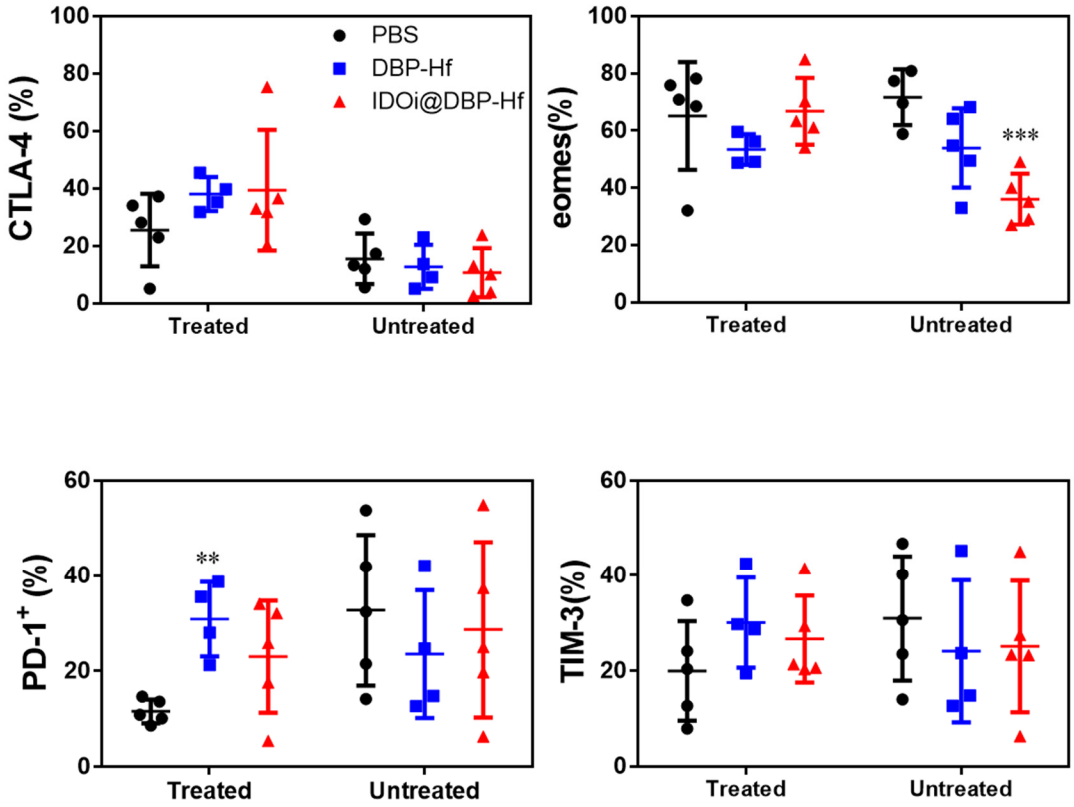

Supplementary Figure 45: Expression of exhausted markers in tumour infiltrating CD8$^+$ T cells in primary and distant tumours. N=5 mice for each group. Centers and error bars denote means and SD, respectively. *P* values were calculated in two-tailed t-test between treatment groups and PBS. *: $P < 0.05$ from control; **: $P < 0.01$ from control.

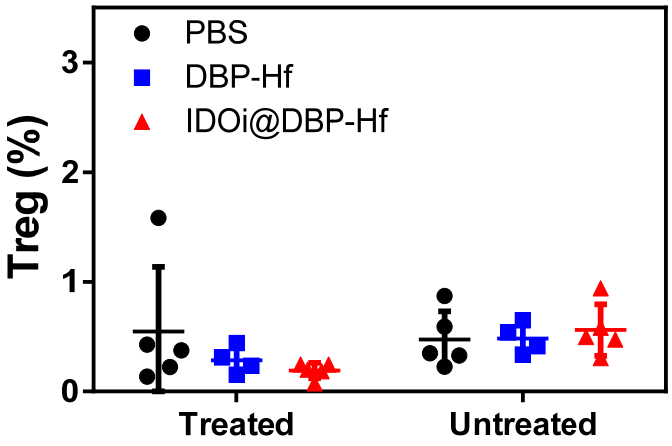

Supplementary Figure 46: Percentage of regulatory $CD4^+$ T cells in total tumour cells. Regulatory $CD4^+$ T cells were gated on $Foxp3^+CD4^+CD3^+CD45^+PI^-$ cells. N=5 mice for each group. Centers and error bars denote means and SD, respectively.

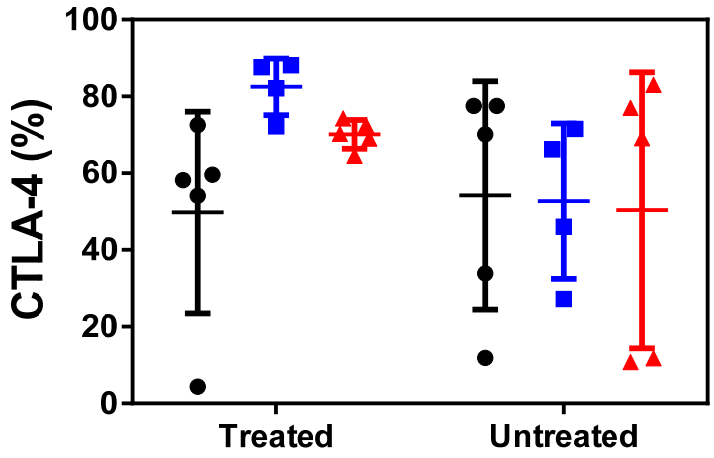

Supplementary Figure 47: CTLA-4 expression on tumour infiltrating CD4$^+$ T cells. N=5 mice for each group. Centers and error bars denote means and SD, respectively.

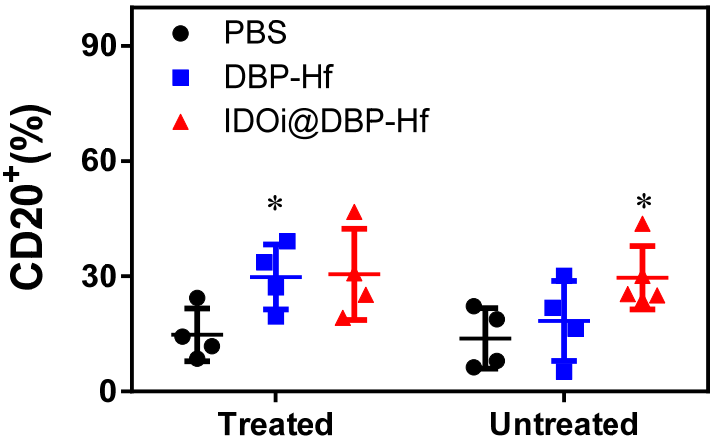

Supplementary Figure 48: CD20 expression in tumour infiltrating B cells. N=5 mice for each group. Centers and error bars denote means and SD, respectively. *P* values were calculated in two-tailed t-test between treatment groups and PBS. *: $P < 0.05$ from control.

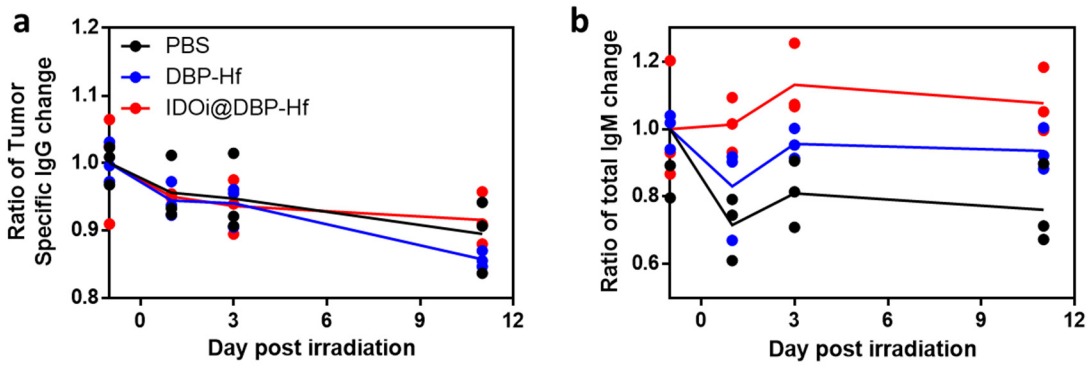

Supplementary Figure 49: Normalized tumour specific IgG change (a) and total IgM change (b) in plasma. Data from D1, D3, and D11 post irradiation were normalized with data from 1 day before irradiation. N=3 mice for each group.

Supplementary Table 1: Constitution analysis of DBP-Hf.

	Hf wt%	H_2DBP wt%	AcOH:DBP by NMR	Formula
1	33.2	56.6	0.56	$Hf_{12}(\mu_3\text{-}O)_8(\mu_3\text{-}OH)_8(\mu_2\text{-}OH)_6(DBP)_{6.6}(AcO)_{3.7}(OH)_{1.1}(OH_2)_{1.1}$
2	32.1	57.5	0.40	$Hf_{12}(\mu_3\text{-}O)_8(\mu_3\text{-}OH)_8(\mu_2\text{-}OH)_6(DBP)_{7.0}(AcO)_{2.8}(OH)_{1.2}(OH_2)_{1.2}$
3	32.9	57.6	0.52	$Hf_{12}(\mu_3\text{-}O)_8(\mu_3\text{-}OH)_8(\mu_2\text{-}OH)_6(DBP)_{6.8}(AcO)_{3.5}(OH)_{0.9}(OH_2)_{0.9}$

Supplementary Table 2: Crystallographic information of TBP-Hf.

Name	TBP-Hf
Formula	$Hf_6(\mu_3\text{-}O)_4(\mu_3\text{-}OH)_4(OH)_4(H_2O)_4(TBP)_2$
Fw	2916.67 g/mol
Temperature (K)	100
Wavelength (Å)	0.61992
Crystal system	cubic
Space group	*P6/mmm*
a, Å	42.194(11)
b, Å	42.194(11)
c, Å	16.960(5)
α, °	90
β, °	90
γ, °	9120
V, Å^3	26150(16)
Z	3
Density (calcd. g/cm^3)	0.552
Absorption coeff. (mm^{-1})	1.253
F(000)	4104
θ range data collection	2.228 – 17.878
Limiting indices	-35<=h<=42 -42<=k<=39 -8<=l<=16
Reflection collected	99934
Independent reflections	5149
R(int)	0.0966
Data/restraints/parameters	5149/27/131
Goodness-of-fit on F^2	1.064
Final R indices [I>2σ(I)]	R1=0.1331, wR2=0.3292
R indices (all data)	R1=0.1463, wR2=0.3429

Supplementary Table 3: Z-average, Number-average, and PDI of DBP-Hf and TBP-Hf dispersed in ethanol.

	Z-average(nm)	Number-average(nm)	PDI
DBP-Hf in ethanol	106.1	72.30	0.103
TBP-Hf in ethanol	103.8	72.72	0.085

Supplementary Table 4: *In vitro* RT-RDT cytotoxicity of DBP-Hf (0.83 μM) and TBP-Hf (1.67 μM) upon X-ray irradiation against different cancer cell lines and comparisons to light induced PDT cytotoxicity. Numbers listed in the table are cell viability (%) compared to PBS-treated cells without X-ray or light irradiation. N=4 biologically independent samples for DBP-Hf experiments and N=3 biologically independent samples for TBP-Hf experiments. The results were reported in mean ± SD.

DBP-Hf					
Tumour Type	Cell Line	0.5 Gy	1 Gy	180 J/cm^2	**X-ray needed[a]**
HNSCC	SQ20B	25.9±2.9	19.5±2.4	44.4±3.2	**0.30**
	JSQ3	42.3±6.4	23.8±6.0	70.8±9.2	**0.20**
	SCC61	32.1±2.1	18.9±2.1	67.9±5.8	**0.13**
	HNSCC135	33.2±4.8	18.7±2.5	62.1±7.6	**0.18**
GBM	U251	43.8±1.8	38.0±1.6	67.1±0.4	**0.16**
	U87MG	18.9±2.7	11.5±2.9	57.0±0.2	**0.17**
Colon	HT29	18.3±0.7	10.1±2.4	39.4±5.6	**0.17**
OCa	A2780cisR	23.9±2.5	15.4±2.1	42.2±4.7	**0.16**
Breast	MCF-7	42.1±2.0	36.2±0.9	58.9±2.7	**0.16**
PDAC	BxPC-3	67.5±1.2	57.5±2.2	74.4±4.8	**0.17**
TBP-Hf					
Tumour Type	Cell Line	0.5 Gy	1 Gy	180 J/cm^2	**X-ray needed[a]**
HNSCC	SQ20B	37.5±7.2	28.5±2.4	68.5±7.1	**0.19**
GBM	U251	63.1±3.4	51.7±4.2	58.7±6.1	**0.67**
	U87MG	63.6±2.7	50.0±1.6	57.4±5.0	**0.65**
	GL261	70.3±1.3	54.7±2.1	60.3±9.2	**0.78**
Colon	CT26	56.8±2.5	43.9±1.5	54.5±7.0	**0.53**
Breast	TUBO	54.7±4.0	44.8±1.7	53.9±3.8	**0.54**
PDAC	TRAMP-C2	69.7±2.0	52.1±0.5	70.3±2.4	**0.45**

[a] X-ray dose (Gy) needed to achieve similar cytotoxicity as 180 J/cm^2 light irradiation (clinically used irradiation dose for PDT).

Supplementary Table 5: Fitting results of the CT26 dose-response curves. The data were fitted with the following function: $F(D) = \exp(-\alpha D - \beta D^2)$. The 10% survival dose (D_{10}), 20% survival dose (D_{20}) and 50% survival dose (D_{50}) are obtained by interpolation from the fit curves. REF's were calculated by dividing D_{10} of PBS with that of test groups.

	α	β	Adj. r^2	α/β	D_{10}	D_{20}	D_{50}
PBS	0.02512	0.01585	0.993	1.58	11.29	9.32	5.87
HfO_2	0.02416	0.01696	0.991	1.42	10.96	9.06	5.72
DBA-Hf	0.3055	0.0033	0.995	92.6	7.01	5.00	2.22
DBP-Hf	0.512	-0.00715	0.993	-71.6	4.82	3.3	1.38

Supplementary Table 6: Fitting results of the SQ20B dose-response curves. The data was fitted with the following function: $F(D) = \exp(-\alpha D - \beta D^2)$. For DBA-Hf, the β value is too low that we change the model to mono-component exponential decay function $F(D) = \exp(-\alpha D)$. The 10% survival dose (D_{10}), 20% survival dose (D_{20}) and 50% survival dose (D_{50}) are obtained by interpolation from the fit curves. REF's were calculated by dividing D_{10} of PBS with that of test groups.

	α	β	Adj. r^2	α/β	D_{10}	D_{20}	D_{50}
PBS	0.1546	0.0058	0.98	26.6	10.64	8.01	3.91
HfO_2	0.2369	0.00306	0.98	77.4	8.73	6.28	2.82
DBA-Hf	0.3598	/	0.99	/	6.4	4.47	1.93
DBP-Hf	0.5061	-0.00901	0.99	-56.2	4.99	3.38	1.4

Supplementary Table 7: Fitting results of the Hela dose-response curves. The data was fitted with the following function: $F(D) = \exp(-\alpha D - \beta D^2)$. The 10% survival dose (D_{10}), 20% survival dose (D_{20}) and 50% survival dose (D_{50}) are obtained by interpolation from the fit curves. REF's were calculated by dividing D_{10} of PBS with that of test groups.

	α	β	Adj. r^2	α/β	D_{10}	D_{20}	D_{50}
PBS	0.07104	0.00528	0.997	13.5	15.21	11.98	6.56
HfO_2	0.0951	0.00534	0.97	17.8	13.68	10.6	5.56
DBA-Hf	0.1719	0.00495	0.99	34.7	10.32	7.66	3.64
DBP-Hf	0.4137	-0.00759	0.98	-54.5	6.29	4.22	1.73

Supplementary Table 8: Fitting results of the TUBO dose-response curves. The data was fitted with the following function: $F(D) = \exp(-\alpha D - \beta D^2)$. For DBA-Hf, the β value is too low that we change the model to mono-component exponential decay function $F(D) = \exp(-\alpha D)$. The 10% survival dose (D_{10}), 20% survival dose (D_{20}) and 50% survival dose (D_{50}) are obtained by interpolation from the fit curves. REF's were calculated by dividing D_{10} of PBS with that of test groups.

	α	β	Adj. r^2	α/β	D_{10}	D_{20}	D_{50}
PBS	0.05004	0.00771	0.98	6.49	14.34	11.56	6.78
HfO_2	0.129	0.00338	0.99	38.2	13.25	9.91	4.78
DBA-Hf	0.2624	/	0.99	/	8.78	6.13	2.64
DBP-Hf	0.5677	-0.00676	0.993	-84	4.27	2.94	1.24

Supplementary Table 9: Fitting results of the JSQ3 dose-response curves. The data was fitted with the following function: $F(D) = \exp(-\alpha D - \beta D^2)$. For DBP-Hf, the β value is too low that we change the model to mono-component exponential decay function $F(D) = \exp(-\alpha D)$. The 10% survival dose (D_{10}), 20% survival dose (D_{20}) and 50% survival dose (D_{50}) are obtained by interpolation from the fit curves. REF's were calculated by dividing D_{10} of PBS with that of test groups.

	α	β	Adj. r^2	α/β	D_{10}	D_{20}	D_{50}
PBS	0.03676	0.00699	0.993	5.26	15.71	12.77	7.67
HfO_2	0.08438	0.00372	0.98	22.7	16	12.35	6.41
DBA-Hf	0.17188	0.00725	0.98	23.7	9.55	7.19	3.51
DBP-Hf	0.41777	/	0.99	/	5.51	3.85	1.66

Supplementary Table 10: Z-average, Number-average, and PDI of DBP-Hf dispersed in ethanol and water and DBP-Hf@PEG dispersed in water.

	Z-average(nm)	Number-average(nm)	PDI
DBP-Hf in ethanol	106.1	72.30	0.103
DBP-Hf in water	n.d.	n.d.	1.000
DBP-Hf@PEG (1:1)[a]	148.6	112.4	0.136
DBP-Hf@PEG (1:2)[a]	136.6	103.0	0.123
DBP-Hf@PEG (1:5)[a]	150.5	103.7	0.146
DBP-Hf@PEG (1:10)[a]	140.7	99.90	0.112

[a] weight ratio of nMOF to DSPE-PEG_{2000}.

Supplementary Table 11: Z-average, Number-average, and PDI of DBP-Hf@PEG dispersed in PBS.

	Z-average(nm)	Number-average(nm)	PDI
DBP-Hf@PEG (1:1)[a]	111.0	75.19	0.148
DBP-Hf@PEG (1:2)[a]	103.8	68.47	0.109
DBP-Hf@PEG (1:5)[a]	107.1	74.65	0.094
DBP-Hf@PEG (1:10)[a]	105.9	70.47	0.105

[a] weight ratio of nMOF to DSPE-PEG_{2000}.

Table S12.
IDOi levels in IDOi@DBP-Hf injected tumours, distant tumours and blood.

	injected tumour	distant tumour	blood
mouse 1	137 ppb	<10 ppb*	<10 ppb*
mouse 2	126 ppb	<10 ppb*	<10 ppb*
mouse 3	126 ppb	<10 ppb*	<10 ppb*

*The LC-MS detection limit is 10 ppb.

Supplementary Table 13: Clinical chemistry of rats after four weekly subcutaneous injections of PBS or DBP-Hf (63 mg/kg). N=6 rats in each group.

Males: Day 29

PBS	**GLU (mg/dL)**	**BUN (mg/dL)**	**CRE (mg/dL)**	**PHOS (mg/dL)**	**AST (U/L)**	**ALT (U/L)**
	102	24	0.4	9.2	125	58
	117	26	0.4	-	122	-
	97	24	0.4	8.7	171	55
	118	36	0.4	9.4	113	65
	105	27	0.5	10	257	101
	110	24	0.5	9.6	98	47
Mean	108	27	0.4	9.4	148	65
SD	8	5	0.1	0.5	59	21

63 mg/kg	**GLU (mg/dL)**	**BUN (mg/dL)**	**CRE (mg/dL)**	**PHOS (mg/dL)**	**AST (U/L)**	**ALT (U/L)**
	111	26	0.4	10.9	107	52
	95	20	0.4	9.7	89	48
	100	27	0.4	11.1	146	49
	96	23	0.4	11.7	105	54
	118	19	0.4	9.9	86	40
	150	23	0.5	16.2	145	55
Mean	112	23	0.4	11.6	113	50
SD	21	3	0.0	2.4	27	5

Females: Day 29

PBS	**GLU (mg/dL)**	**BUN (mg/dL)**	**CRE (mg/dL)**	**PHOS (mg/dL)**	**AST (U/L)**	**ALT (U/L)**
	116	27	0.6	9.9	107	55
	116	20	0.6	8.7	95	45
	107	22	0.5	7.9	96	36
	93	24	0.6	8.7	110	45
	118	21	0.5	8.5	108	64
	107	26	0.6	8.6	100	38
Mean	110	23	0.6	8.7	103	47
SD	9	3	0.1	0.7	7	11

63 mg/kg	**GLU (mg/dL)**	**BUN (mg/dL)**	**CRE (mg/dL)**	**PHOS (mg/dL)**	**AST (U/L)**	**ALT (U/L)**
	114	22	0.4	9.3	106	39
	95	22	0.6	9.9	107	48
	94	23	0.6	8.7	78	29
	111	21	0.4	9.2	106	38
	105	17	0.6	8.7	98	41
	104	24	0.5	-	106	30
Mean	104	22	0.5	9.2	100	38
SD	8	2	0.1	0.5	11	7